The Thesis Committee for Mahesh Venkatesan
Certifies that this is the approved version of the following thesis:

Experimental and theoretical analysis of a novel vertical axis wind turbine with solar cell integration

APPROVED BY
SUPERVISING COMMITTEE:

Supervisor:

Halil Berberoglu

Yaguo Wang

Experimental and theoretical analysis of a novel vertical axis wind turbine with solar cell integration

Mahesh Venkatesan, B.Tech

Thesis

Presented to the Faculty of the Graduate School of

The University of Texas at Austin

in Partial Fulfillment

of the Requirements

for the Degree of

Master of Science in Engineering

The University of Texas at Austin

May, 2014

Dedication

Dedicated to my parents for their steadfast encouragement

Acknowledgements

First, I would like to acknowledge the support of *Renewable Energy Solutions LLC* towards this study. I would like to express my sincere thanks to Onur Taylan of the Solar Energy and Renewable Fuels Laboratory for his truly invaluable expertise and guidance in this research. I would also like to thank the current and former members of the Solar Energy and Renewable Fuels Laboratory for a friendly and comfortable lab environment: Dr. Thomas Murphy, Akhil Kulkarni, Babak Nasouri, Cody Bond, David Navar, Daniel Campbell, Joey Anthony, Daniel Pinero and Luis Galindo.

I would like to express my gratitude to Bharadwaj Muralidharan and Vaidyanathan Krishnamurthy for sharing their expertise on Electrical engineering. I would like to acknowledge Varun Devarajan, Vikram Devarajan and Kaushik Subramanian for making my stay in Austin a comfortable and memorable one.

Last but not least, I would like to express my sincere gratitude to my advisor Dr. Halil Berberoglu for his guidance and encouragement to achieve the best of my potential.

Abstract

Experimental and theoretical analysis of a novel vertical axis wind turbine with solar cell integration

Mahesh Venkatesan, M.S.E.

The University of Texas at Austin, 2014

Supervisor: Halil Berberoglu

There has been an increased interest in renewable energy systems in recent years as a result of concerns on depleting fossil fuel reserves and climate change. Wind and solar energy are amongst the most popular renewable energy technologies. In order to use the full or maximum possible extent of a renewable energy resource in a region, hybrid systems extracting wind and solar energy simultaneously are a popular and obvious choice.

It is desired to design hybrid systems that enhance the renewable energy output without increasing the foot print area compared to the base case of only wind or only solar energy. One potential way forward is to consider a vertical axis wind turbine with an enhanced surface area which can be used for mounting solar cells. This way the foot print area remains the same while both wind and solar power are obtained

simultaneously. *Renewable Energy Solutions LLC* has manufactured a novel 2 m high and 2 m in diameter vertical axis wind turbine called *Marilyn* which has an enhanced surface area, which can be used for the aforementioned purpose.

This thesis focuses on the development of a hybrid solar-wind turbine design based on the Marilyn system. Firstly, the wind and solar resource was assessed at Austin, TX using weather monitoring instruments. Typical Meteorological Year 3 (TMY3) data was also used in conjunction with the measured data to estimate the wind and solar resource at Austin, TX.

Secondly, the wind turbine performance was assessed based on whether is it able to achieve grid tie in for wind power production starting at wind speeds of 3-4 m/s. It was found that replacing the current generator with different model featuring higher voltage output at lower rotational speeds could help achieve this. Based on this suggested replacement and using the wind resource data, the yearly wind energy production was estimated to be 240 kWh.

Finally, a theoretical analysis was performed for estimating the yearly solar energy production. A base case analysis was first made on power production on a particular day of the year if only the top portion of every alternate face of the turbine is covered with flexible 3.4 % efficient solar cells. This analysis is subsequently extended to the case when flexible 20 % efficient solar cells cover the entire top surface of the turbine and the corresponding conservative yearly solar energy output was estimated to be 310 kWh. Thus the total yearly energy output from the *Marilyn* hybrid system is 550 kWh, which is around 5 % of the annual electricity usage of a typical American home

Table of Contents

List of Tables

List of Figures

Chapter 1: Introduction

With concerns on depleting fossil fuels and climate change, interest in renewable environmental friendly energy sources have been picking up in the recent years. Global renewable energy demand continued to rise in 2011 to 2012, supplying 19 % of the energy consumption in 2011 [1]. Wind and solar energy are amongst the most promising renewable energy technologies. Globally, wind power accounted for about 39% of renewable power capacity added in 2012, followed by solar photovoltaic systems, accounting for approximately 26% [1].

The current annual residential electricity consumption in the United States is estimated to be 10, 837 kWh [2] and assuming all this comes from use of fossil fuels, the associated carbon foot print is estimated to be 74 tons of CO2 [3]. The use of small scale vertical axis wind turbines (of up to 10 kW nominal power output) is increasingly being considered to augment the power supply and to reduce the carbon footprint for residential homes, sailing boats and remote locations such as telecommunication towers [4], [5], [6]. These use permanent magnet generators (PMGs) which are direct driven, without the need for a gear box thereby resulting in high reliability and reduced maintenance costs [6]. In particular, this technology is even more appealing to remote telecommunication towers where the remoteness of the location makes transport of fuel for conventional electrical generators quite cost intensive [4]. To make the renewable power supply more reliable throughout the year, the idea of supplementing the wind power with solar power from installing solar panels has been considered [4], [7]. However the installation of the

solar panels increases the foot print area of the set up. This can prove to be a problem in residential applications where space constraints are fairly common.

In this study, we consider a novel vertical axis wind turbine named *Marilyn* manufactured by *Renewable Energy Solutions, LLC*. This turbine has an enhanced surface area and one of the potential ways to put this to use is by mounting solar cells on it to obtain solar power simultaneously with wind power. This ensures that on the same foot print area, wind and solar power is obtained simultaneously. Also the rotation of the turbine, ensures that the solar cells are cooled by convection of the air flow and are also kept clean of dirt which can reduce the irradiance on the solar cells [8]. We aim to estimate the average annual wind and solar energy production from this hybrid system.

Firstly the wind and solar resource is estimated real time with weather monitoring instruments and also using statistical Typical Meteorological Year 3 (TMY3) data. Next, based on observations, a recommendation is made on the current generator used with the wind turbine and a yearly estimate on the wind energy production is made with the suggested generator and the wind resource data.

Finally, a theoretical estimate is made on the yearly solar energy production if the entire top surface of the turbine is covered with flexible 20 % efficient CIGS (Cadmium Indium Gallium Sulphide) solar cells and this is shown to be on the same order as that of the wind energy production.

Chapter 2: Current State of Knowledge

2.1 WIND ENERGY SYSTEMS

Wind turbines are classified as horizontal axis and vertical axis wind turbines.

Horizontal axis wind turbines have the axis of rotation of the turbine horizontal, while vertical axis wind turbines have the axis of rotation vertical. Horizontal axis wind turbines have a lower starting torque requirement, do not stall in gusty winds and are capable of operating at the optimum point to produce maximum power for an extended period of time. Their typical heights of 50 m or more allow them to capture the higher wind speeds at high altitudes. Their main disadvantages are that they require an orientation mechanism to point them in the wind direction and their maintenance is expensive because of their substantial height [4], [6], [9].

Vertical axis wind turbines are able to capture wind from all directions and are also called omni directional. This eliminates the need for an orientation mechanism making them useful in locations where wind direction fluctuates considerably. The generator is at ground level facilitating easy maintenance. Their low rotational speed however leads then to having a higher starting torque and a lower efficiency of conversion of wind energy to useful power. Also, the high torque fluctuations with each rotation result in a higher chance of structural failure by fatigue [4], [6], [9].

Vertical axis turbines are broadly classified as Savonius turbines (with vertically mounted airfoils), Darrieus type (with straight or bent blades) and the straight bladed H rotor. Figure 2.1 illustrates the types of vertical axis wind turbines [9].

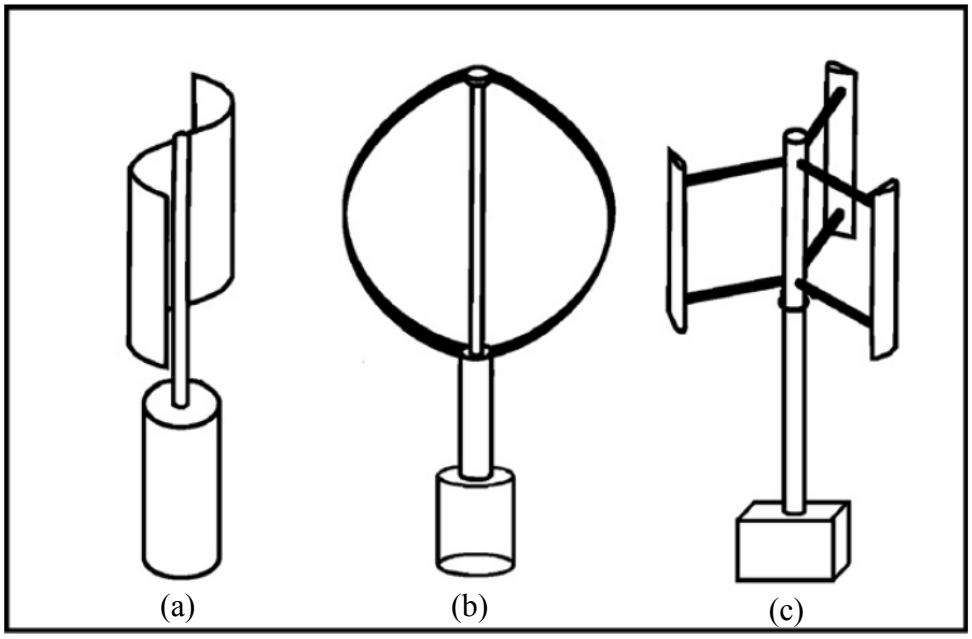

Figure 2.1: Types of vertical axis wind turbines: (a) Savonius, (b) Darrieus and (c) H-rotor [9].

The mechanical power, P that can be produced by a wind turbine can be found from [6], [10]

$$P = \frac{1}{2} C_P \rho A V_{wind}^3 \tag{2.1}$$

where C_P is the power coefficient, ρ is the density of the air, A is the swept area of the turbine and V_{wind} is the wind speed. The power coefficient represents the aerodynamic efficiency of the wind turbine and is a function of the tip speed ratio, λ, which is defined as [6], [10]

$$\lambda = \frac{R\omega}{V_{wind}} \tag{2.2}$$

where ω is the rotational frequency of the turbine, R is the turbine radius and V_{wind} is the wind speed.

The theoretical maximum for C_P is 0.5926 called the Bethz Limit [6], [10]. This implies that a theoretical upper limit exist on the efficiency of conversion of wind energy to mechanical energy for a wind turbine.

Figure 2.2 shows the variation of power coefficient with tip speed ratio for various types of horizontal axis and vertical axis wind turbines [11].

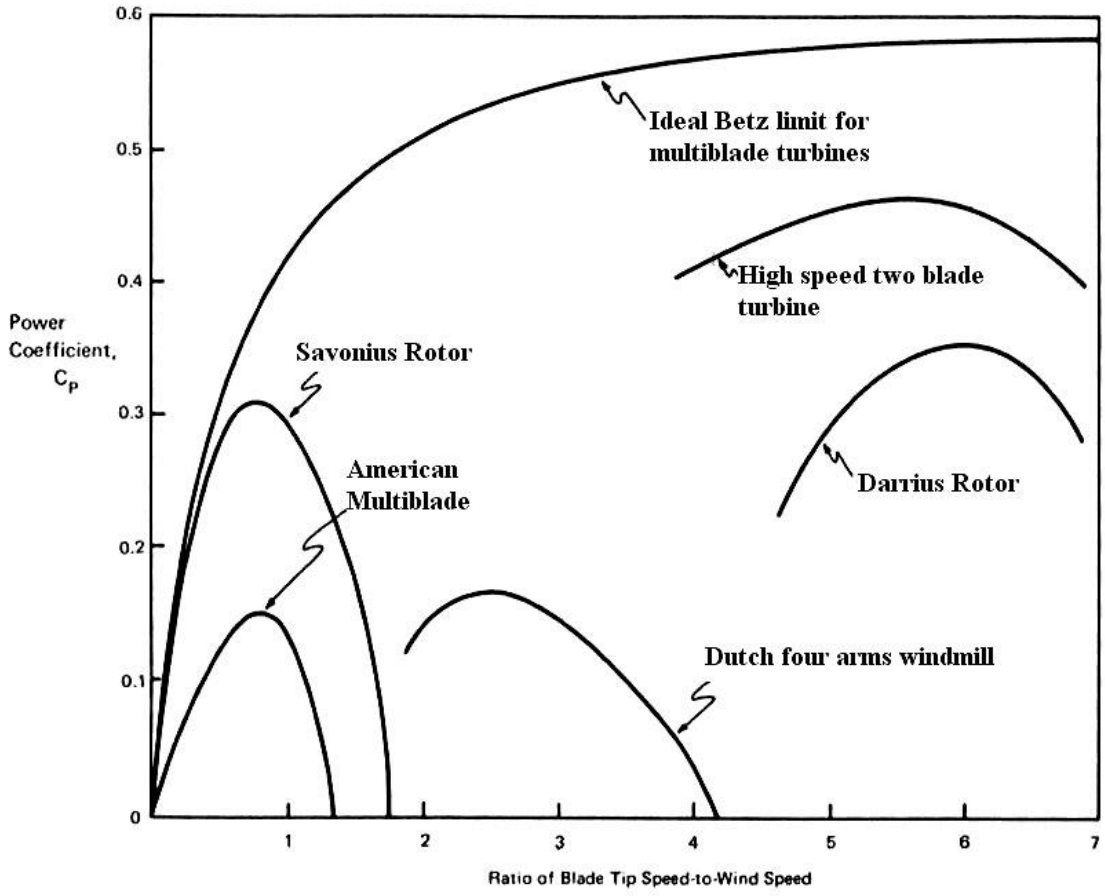

Figure 2.2: Power coefficient with tip speed ratio for different classes of wind turbines [11].

The largest horizontal axis wind turbine currently installed is the Vestas V164 8 MW in Denmark with a rotor radius of 80 m [12]. The largest vertical axis wind turbines the EOLE C 4.2 MW installed in Canada [6]. The Alta wind energy farm in California, USA is the largest onshore wind farm in the world with a capacity of 1020 MW [13].

Small scale power generation systems using vertical axis wind turbines that generate 0.5 -1 kW using direct drive gearless permanent magnet generators have been analysed and developed by Bumby *et al* [5].

2.2 SOLAR ENERGY SYSTEMS

Solar energy systems are broadly classified as solar thermal systems and solar photovoltaic systems [10] :

Solar thermal systems focus on converting solar energy to thermal energy which can be used for water heating or even power generation using Rankine cycles. The solar radiation is typically concentrated by parabolic mirrors for power generation applications [10]. The largest solar thermal facility at present is the 392 MW Ivanpah facility in the Mojave desert, California USA [1].

Photovoltaic systems use solar cells that convert solar energy directly to electricity [10]. The largest operational solar photovoltaic project is the Agua Caliente project in Yuma county, Arizona USA with a capacity of 250 MW [14].

For the purposes of this study, it is useful to elaborate on the characteristics of the solar cells. A typical solar cell is characterized by its current-voltage and power-voltage curves as shown in Figure 2.3 [10] [15].

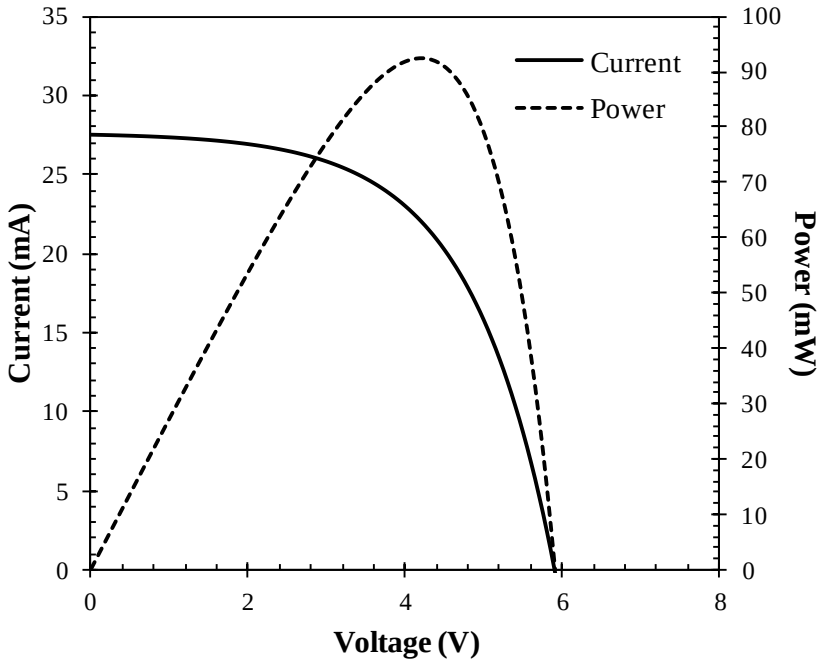

Figure 2.3: Current-voltage and power-voltage curves of the *Powerfilm SP4.2-37* solar cell at one sun irradiation [10] [15].

The current at zero voltage is referred to as short circuit current Isc and the voltage at open circuit is referred to as open circuit voltage Voc. From Figure 2.3, there is particular current and voltage setting at which the power output becomes maximum. This point is referred to as the Maximum Power Point (MPPT) and the power rating of the solar cells is specified at this point. The current-voltage and the power-voltage curves are typically rated at 1000 W/m2 solar irradiation referred to as one sun [10], [15] .

2.3 WIND SOLAR HYBRID SYSTEMS

Hybrid systems that achieve simultaneous production of wind and solar energy typically achieve this by using a horizontal or vertical axis wind turbine and a separate solar energy system in the form of solar cell arrays [7] [16]. The typical drawback with such systems is that the installation of the solar panels near the wind turbine results in the foot print area being increased three to four times. Ranaboldo *et al* [16] have considered wind solar hybrid off grid systems to electrify rural communities in Cape Verde by using 210, 2100 and 4200 W solar panels in conjunction with 600, 3500 and 7500 W wind turbines. Assuming typical solar cell efficiencies of 20 % [10], the corresponding increase in fort print area because of the solar panels ranges from 1 to 20 m^2. A similar system in residential areas could run in to problems because of space constraints typical of residential areas.

Thus motivation exists to analyze systems that enhance power production from renewable energy sources with the same foot print area. This study attempts to do that by considering the possibility of mounting solar cells on the surface of a novel vertical axis wind turbine *Marilyn* manufactured by *Renewable Energy Solutions LLC*. The foot print area remains the same and this is the key advantage in environments such as residential housing where space constraints could be an issue.

Chapter 3: Methodology

This chapter describes the experimental setup used and the procedures followed in this study. The first part of the chapter focuses on the collection of weather data using weather monitoring devices and a data acquisition system. The second part describes the wind turbine, its grid connection and power characterization. The third part deals with the solar cells, its theoretical analysis and power characterization.

3.1 DATA COLLECTION BY WEATHER STATION

3.1.1 Weather monitoring instruments

The weather parameters relevant to the analysis are- Global Horizontal Radiation (in W/m^2), Wind Speed (in m/s) and Wind Direction (in degrees measured clockwise from the North). We use a *LI-COR* LI-200 pyranometer to measure the Global Horizontal Radiation, an *Inspeed Vortex* anemometer to measure Wind Speed and an *Inspeed* wind vane to measure the wind direction. Figure 3.1 shows the weather monitoring instruments installed at The Pickle Research Campus, The University of Texas at Austin. Table 3.1illustrates the calibration of these instruments and Table 3.2 shows the uncertainty in the calibration.

Table 3.1: Calibration data of weather monitoring instruments

Weather Instrument	**Calibration data**
LI-COR LI-200 pyranometer	79.2 μA per 1000 W/m^2 [17]
Inspeed Vortex anemometer	2.5 miles per hour (mph) per Hz [18]
Inspeed wind vane	0.25-4.75 V corresponding to 0 and 360° from the North measured clockwise [19]

Table 3.2: Uncertainty in calibration of weather monitoring instruments

Weather Instrument	**Uncertainty in calibration**
LI-COR LI-200 pyranometer	± 5 % [20]
Inspeed Vortex anemometer	0.5 mph from 4 to 10 mph ± 4% from 10 to 50 mph[18]
Inspeed wind vane	± 0.3 to 0.5% [19]

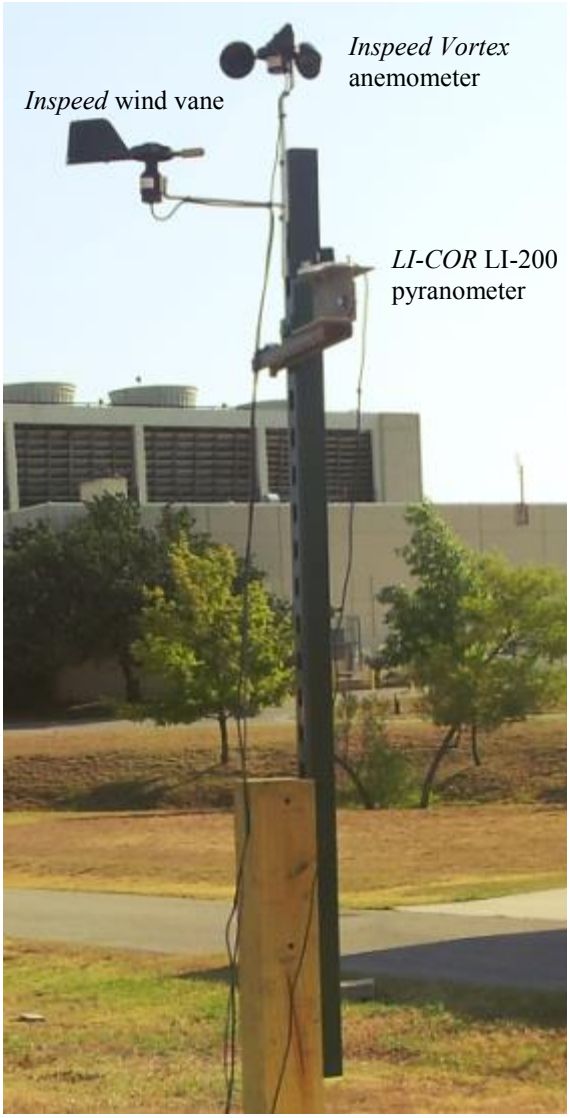

Figure 3.1: Weather monitoring instruments installed at The Pickle Research Campus, The University of Texas at Austin

3.1.2 **Data logger**

The weather instruments in Table 3.1 are connected to a *Campbell Scientific* CR10X data logger which records the data in its inbuilt memory. Figure 3.2 shows the CR10X data logger with the ports labelled

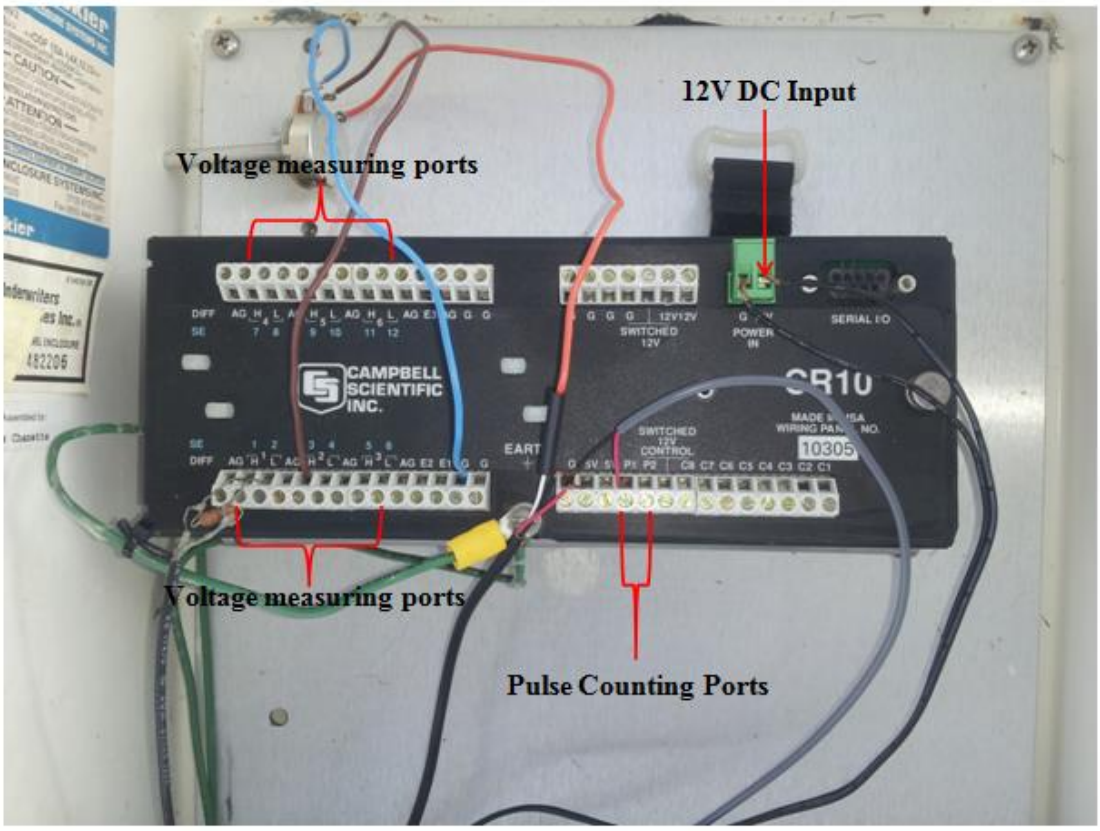

Figure 3.2: *Campbell Scientific* CR10X data logger

Figure 3.2 shows the voltage measuring ports are labelled 1-6, situated on the left hand side. These ports can measure DC voltages of up to 2.5 V [21]. Each of these numbered ports is subdivided into two- H and L signifying High and Low. Thus it is the voltage difference between H and L which is measured.

Figure 3.2 also shows the Pulse Counting Ports P1 and P2 on the right hand side. These ports are capable of counting the electric pulses received per second and thus are capable of measuring the frequency of the electric pulses. Besides, there are two ports that supply 5 V DC and ports labeled G and AG standing for Ground and Additional Ground respectively which are at zero potential [21].

The CR10X requires a DC supply of 12 V for its operation [21]. An adapter that converts 110 V AC to 12 V DC provides this power supply.

3.1.3 **Weather data monitoring and collection**

The next step is to connect the weather monitoring instruments to the CR10X data logger so that their signals can be recorded. We shall deal with the *LI-COR* LI-200 pyranometer first. This gives a current output proportional to the Global Horizontal Radiation as shown in Table 3.1. Since the data logger can measure only DC Voltage or pulse, the current output has to be converted a voltage output. This is achieved by connecting a *Vishay* PTF 120 Ω resistor across the ends of the pyranometer and then connecting both ends of the resistor to the H and L sub ports of port 1 on the CR10X. Figure 3.3 shows the connection of the LI-200 pyranometer to the CR10X data logger

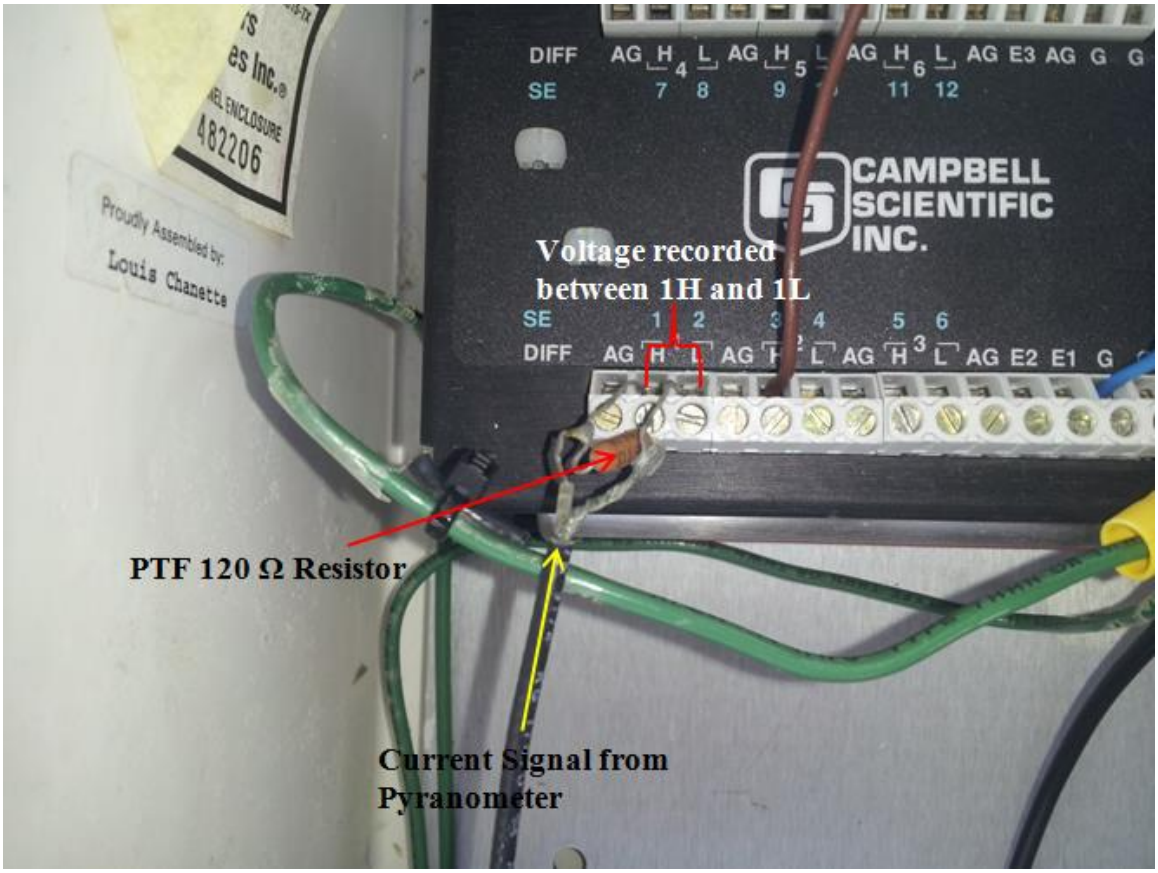

Figure 3.3: *LI-COR* LI-200 pyranometer connection to the CR10X data logger

Since the data logger records voltage, we need to define the calibration of the pyranometer in terms of mV per 1000 W/m^2 of Global Horizontal Radiation. This is achieved by multiplying 79.2 μA by 120 Ω to give 9.504 mV per 1000 W/m^2 of Global Horizontal Radiation.

The *Inspeed Vortex* Anemometer generates electric pulses whose frequency is proportional to the wind speed as shown in Table 3.1. The output of the Anemometer is fed into the pulse port P1of the data logger which records the frequency of the pulses.

The ground wire is plugged into the Ground Port. Figure 3.4 illustrates the connection of the anemometer to the data logger.

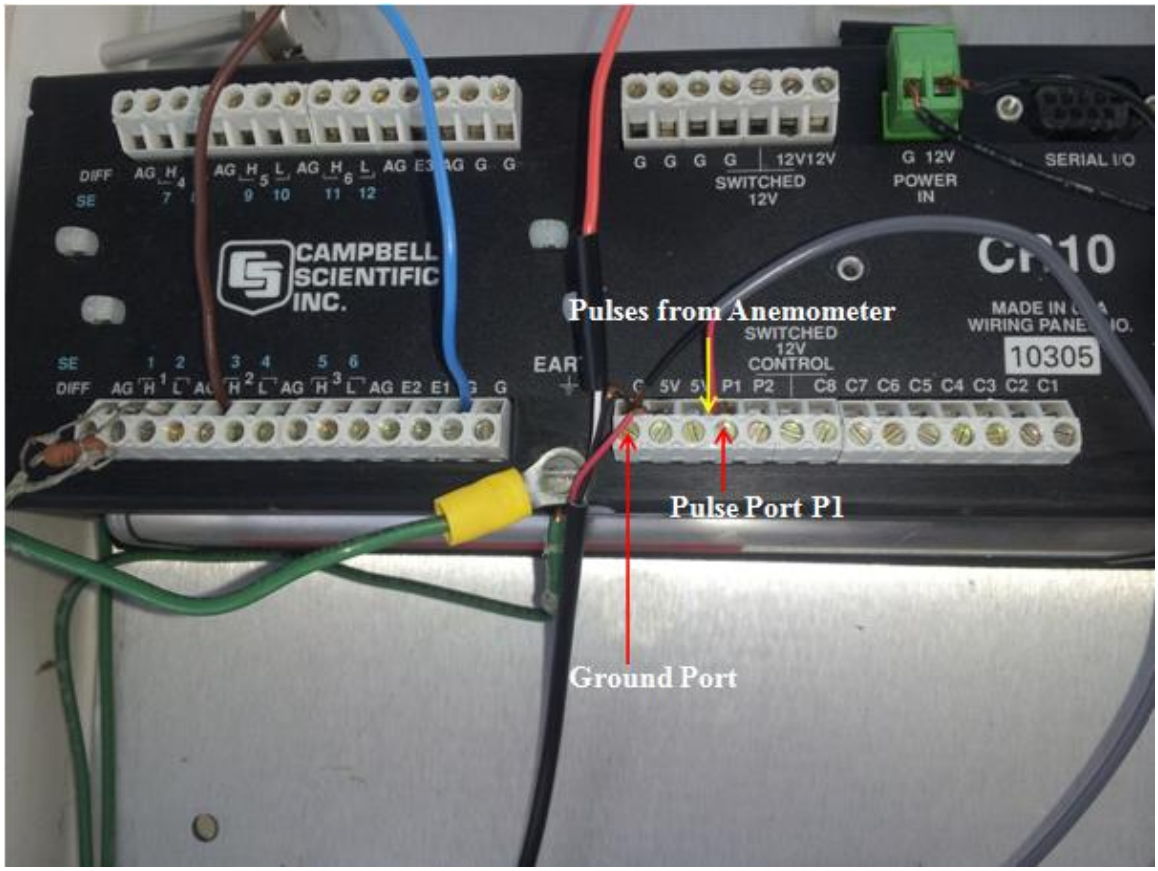

Figure 3.4: *Inspeeed Vortex* anemometer connection to the CR10X data logger

The *Inspeed* Wind Vane requires a 5 V DC supply for operation [19]. The maximum possible voltage that can be generated by the wind vane i.e. 4.75 V is higher than the maximum voltage that can be recorded by a voltage sensing port on the data logger, which is 2.5 V [19], [21]. Thus we use a 1 KΩ resistor as a voltage divider/potentiometer to halve the voltage output of the Wind Vane and this halved voltage is then fed into the voltage sensing port 3H on the data logger. This ensures that

the maximum output to the data logger is 4.75/2= 2.375 V which is less than the maximum measurable value of 2.5 V. Figure 3.5 shows the connection of the wind vane to the data logger.

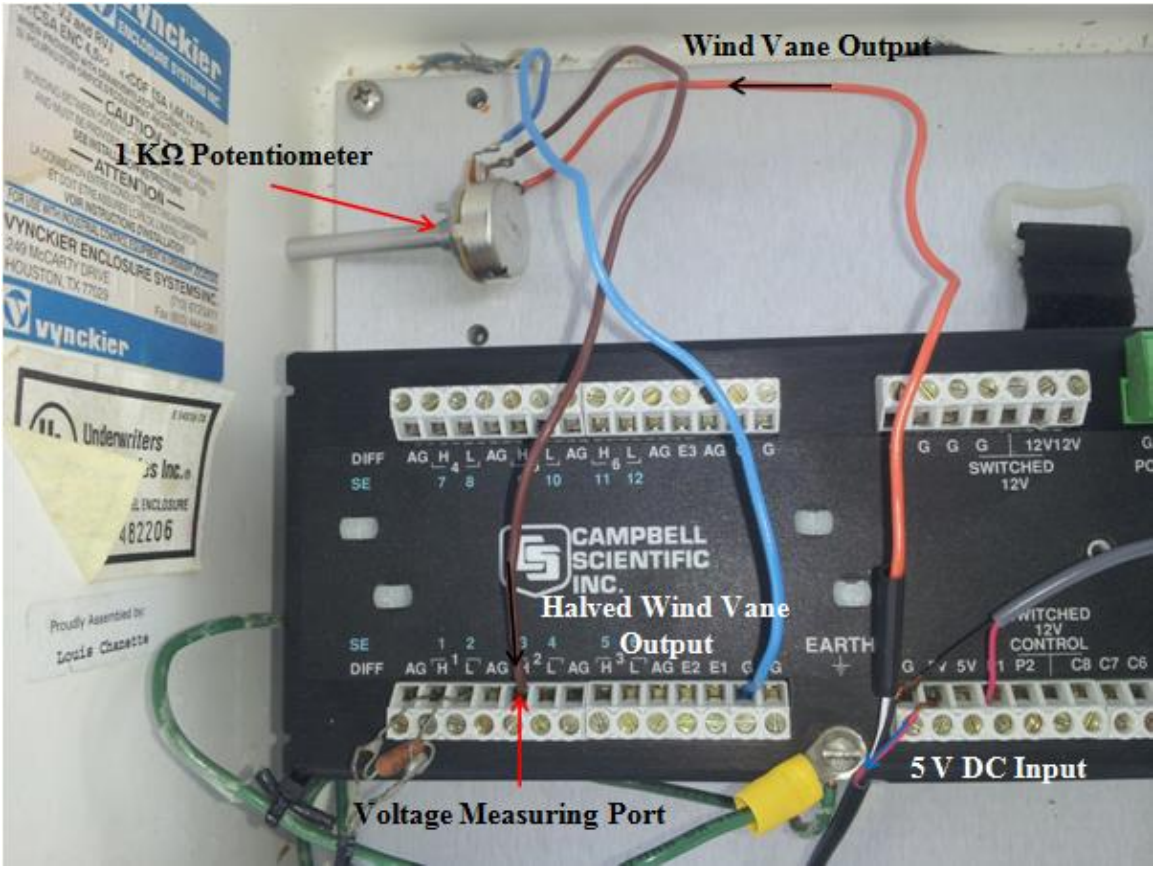

Figure 3.5: *Inspeeed* wind vane connection to the CR10X data logger

The PC200 W software is used to program the data logger to make it record the readings at the respective ports and store it in its memory. The data is periodically retrieved and stored in a dat file which can be then exported to Microsoft Excel. Table 3.3 illustrates the least count of the data, measured on various ports on the data logger

Table 3.3: Least count measured on the ports of the CR10X data logger

Port	To measure	Least count of data recorded
1 (1H-1L)	Global Horizontal Radiation	0.001 mV
3H	Wind Direction	1 mV
P1	Wind Speed	0.001 Hz

3.2 DATA COLLECTION FOR WIND ENERGY

3.2.1 Description of wind turbine and generator

The *Marilyn* 2x2 wind turbine is a vertical axis wind turbine manufactured by *Renewable Energy Solutions, LLC* incorporated in Maryland, USA. It is 2 m in height and 2 m in diameter and made of fiber glass. The wind speed at which rotation begins is 2-3 m/s and at 20 m/s wind speed, the maximum rotational speed of 150 rpm is achieved. The turbine is designed to be aerodynamically self-braking which implies that for wind speeds above 20 m/s, the rotational speed doesn't exceed 150 rpm. The efficiency of conversion of wind energy to rotational motion is claimed to be 30 % and the unique high surface area can potentially be used for solar cell integration to achieve simultaneous wind and solar power collection with the same foot print area [8].

The *Air Boss* 1400-96 V, a direct drive gearless generator manufactured by the *American Renewable Energy Corporation* (AERCO) is used with this turbine without a gearbox to convert rotational motion to electricity.

Figure 3.6 shows the Marilyn 2x 2 wind turbine with the generator and Figure 3.7 shows the voltage and power characteristics of the Air Boss 1400-96 V generator.

Figure 3.6: *Marilyn* 2x 2 wind turbine with the *Air Boss* 1400-96 V generator

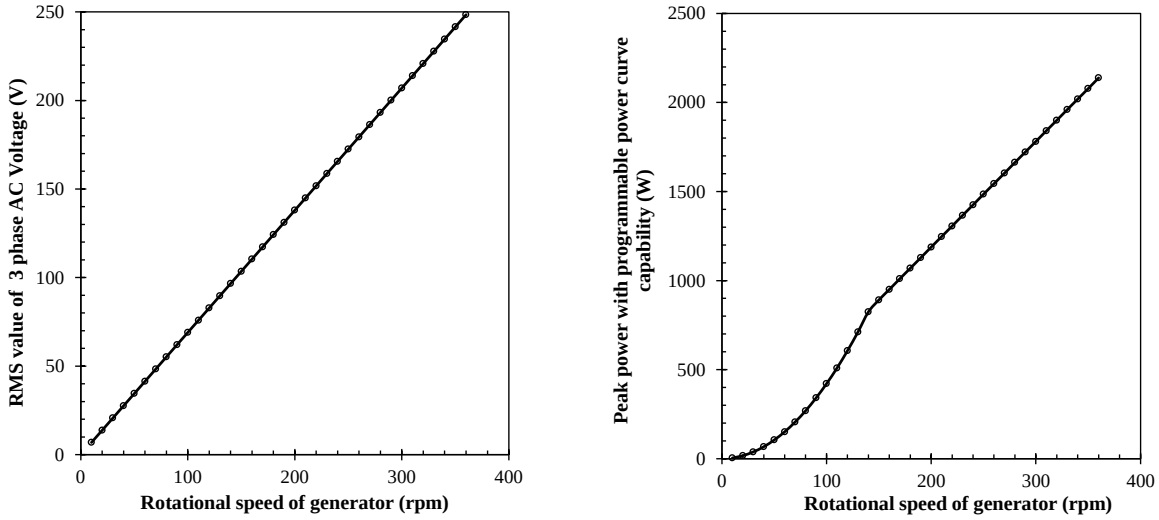

Figure 3.7: *Air Boss* 1400-96 V voltage and power characteristics [22]

3.2.2 **Connection of the turbine-generator system to the grid**

The *Marilyn* 2 x 2 wind turbine and the Air Boss 1400-96 V generator is connected to the *Aurora PVI 2500 Wind Interface* (manufactured by *Power One Inc*) rectifier and the *Aurora PVI-3.0/3.6/4.2-OUTD-OSW* (manufactured by *Power One Inc*) inverter to enable connection to the 3 phase AC grid. Figure 3.8 shows the schematic for the grid connection.

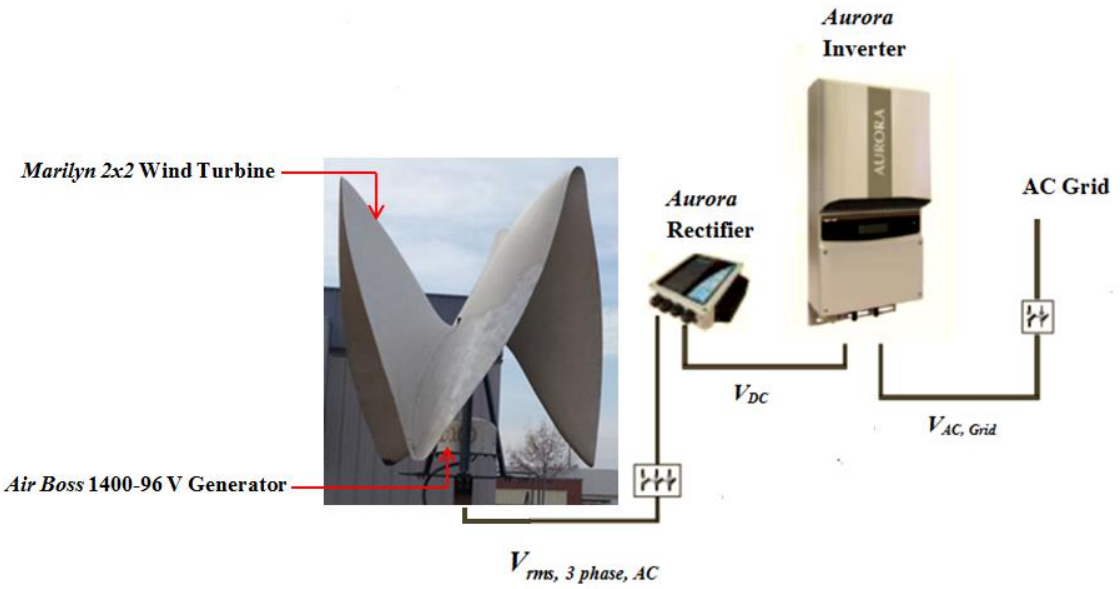

Figure 3.8: Schematic for grid tie in of the *Marilyn* wind turbine and the *Air Boss* 1400-96 V generator

The inverter needs a minimum of 50 V DC input from the rectifier for the grid connection to be activated [23]. In open circuit, the output DC voltage of the rectifier V_{DC} is related to the rms value of the 3 phase input AC voltage $V_{rms,\ 3phase,\ AC}$ as [24]

$$V_{DC} \approx 1.35 V_{rms,3phase,AC} \tag{3.1}$$

In closed circuit, the output DC voltage of the rectifier is 10-20 % less than the value obtained from Equation (3.1) [24].

Thus Equation (3.1) implies that if the minimum voltage output of the rectifier for grid tie in is 50 V, the corresponding minimum rms value of the 3 phase input AC voltage is 37 V.

The relevant data like the input and output voltages and the power exported can be collected from the inverter via USB interface using the *Aurora* Communicator Software [23] .

3.3 DATA COLLECTION FOR SOLAR ENERGY

3.3.1 **Description of solar cells**

Powerfilm 4.2 V, 22 mA SP4.2-37 flexible solar cells are considered for obtaining solar power. Figure 3.9 illustrates the length and width of these solar cells.

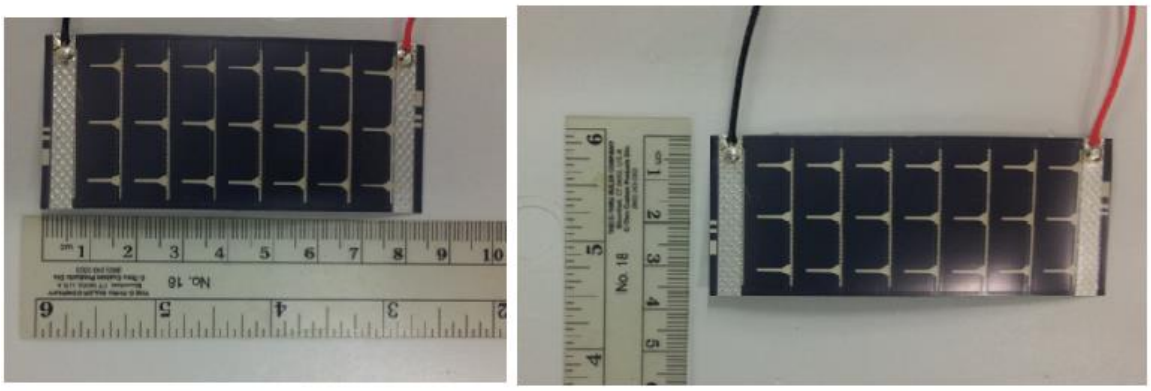

Figure 3.9: Length and width of the *Powerfilm 4.2 V, 22 mA SP4.2-37 solar cells* shown as 8.4 cm and 3.8 cm respectively

The open circuit voltage is 5.9 V and the current and voltage at maximum power point is 4.2 V and 22 mA for these solar cells [15]. These are further elaborated in Section 3.3.3.

3.3.2 **Area selection for solar cells**

Figure 3.10 shows the possible positioning of the *Powerfilm* solar cells on one of the faces of the turbine. The solar radiation intensity decreases from top to bottom, and hence the solar cells are laid from top to bottom length wise. We assume that a curvature of up to 0.007 mm^{-1} can be withstood by these solar cells. The total number of zones from top to bottom containing the solar cells is 29 if we wish to cover as much of the area as we can. Since we are laying the solar cells length wise, the width of each zone is 3.8 cm. The lengths of the zones are integral multiples of the length of a single solar cell i.e. 8.4 cm. Thus for instance if the length of a zone is 16.8 cm it means it has two solar cells laid length wise in it.

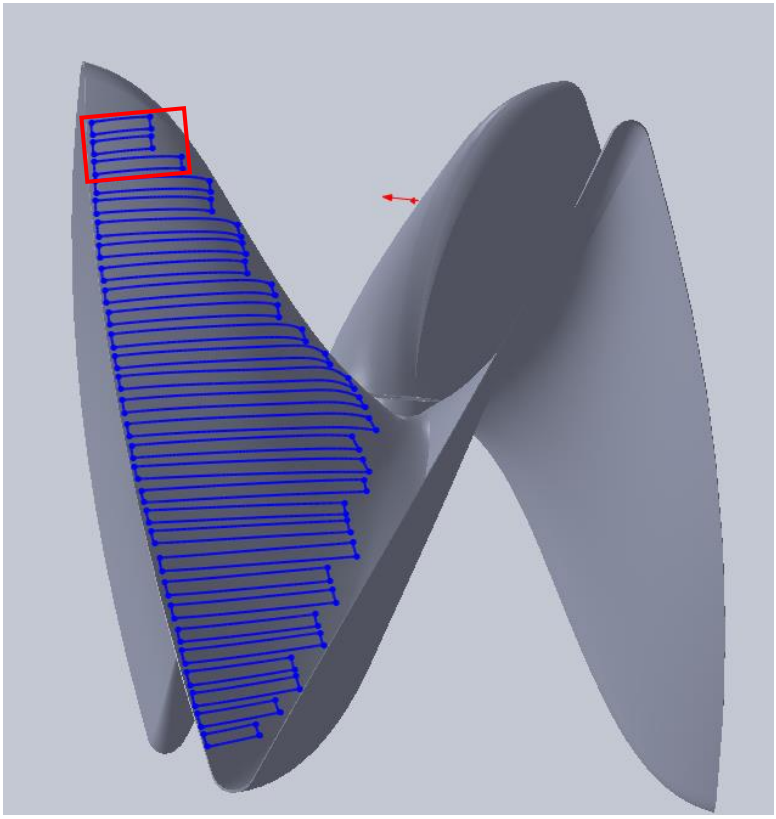

Figure 3.10: Positioning of the Powerfilm solar cells on one of the faces of the Marilyn turbine. Each of the rectangular patches is one zone. The red box is Section 1 which represents the zones chosen to be actually covered with solar cells in our experiment

For the sake of the experiment, we choose the top three zones and collectively label them as Section 1 as Figure 3.10 illustrates. Section 1 has seven solar cells. We plan to use solar cells suffice for Section 1 only on this face of the turbine. We follow the same plan for the other two equivalent faces on the turbine implying that a total of three such sections are used, having seven solar cells each.

Figure 3.11 shows conceptually the process of obtaining power from these solar cells. A slip ring is used to obtain power from these rotating solar cells. The slip ring is

clamped around the rotating shaft. The brushes are held stationary, while the slip ring rotates, thus transmitting power from the solar panels mounted on the rotating turbine

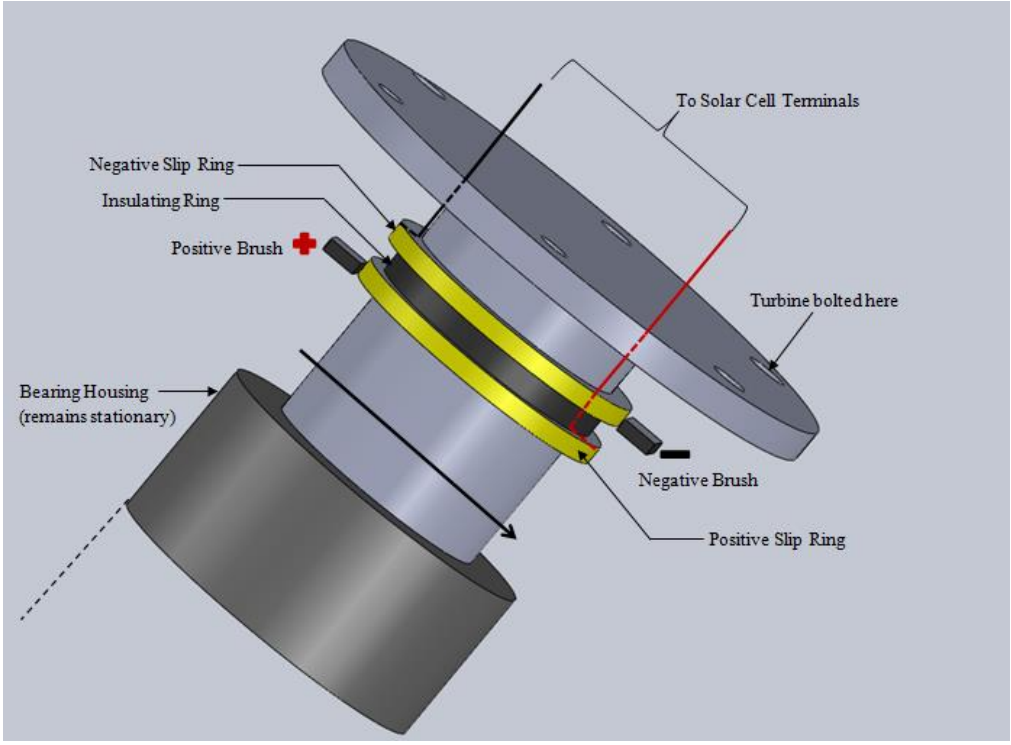

Figure 3.11: Conceptual illustration of a slip ring system to obtain power from the rotating solar cells mounted on the *Marilyn* turbine

Figure 3.12 shows the *SNH090-04s through bore Slip Ring* manufactured by *Senring Co.* installed on the rotating shaft to obtain power from the rotating solar cells.

Figure 3.12: Close up view of the *Marilyn* turbine showing the *Senring* slip ring installed

3.3.3 **Characterization of the solar cells**

Figure 3.13 shows the equivalent circuit of a generic photovoltaic (PV) solar cell. The equivalent circuit of a PV cell consists of a shunt resistance, R_{SH}, a resistance in series, R_S, a diode in parallel to R_{SH} and a voltage source, V. Current I passes through the cell when the cell is connected to a load, R_{load} [25].

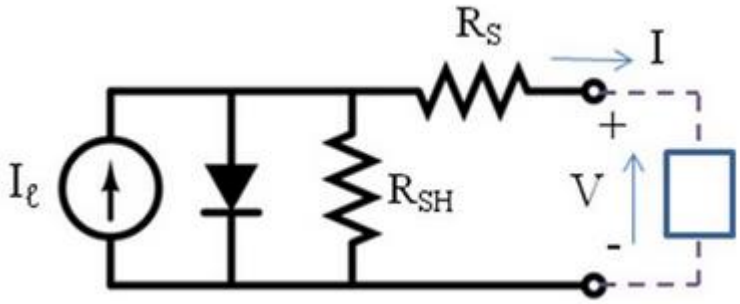

Figure 3.13: Equivalent circuit model for a solar cell [25].

The most general IV characteristic of the solar cell, at 1 sun or 1000 W/m2 irradiation can be described as [10], [25]

$$I = I_l - I_o\left[\exp\left\{\frac{q(V+IR_s)}{nkT}\right\}-1\right]-\frac{V+IR_s}{R_{SH}} \tag{3.2}$$

where I_o is the diode saturation current, n is the diode ideality factor (between 1 and 2), k is the Boltzmann constant, q is the electronic charge and T is the temperature of the cell.

Equation (3.2) can be simplified by assuming an ideal scenario where there are no losses in the solar cell implying that R_{SH} tends to infinity and R_S tends to zero. Additionally, if the current equals the short circuit current I_s at zero voltage and the voltage equals the open circuit voltage V_o at zero current, Equation (3.2) simplifies to,

$$I = I_s\left(1-\frac{e^{\alpha V}-1}{e^{\alpha V_o}-1}\right) \tag{3.3}$$

where

$$\alpha = \frac{q}{nkT} \tag{3.4}$$

It is possible to relate α to the parameters at the maximum power point. At maximum power point, VI is maximum where I is given by Equation (3.3). Differentiating VI with respect to V and setting it to zero results in

$$e^{\alpha V_m}\left(1+\alpha V_m\right)=e^{\alpha V_o} \tag{3.5}$$

If the solar irradiation is different than 1000 W/m^2, say G in W/m^2, Equation (3.3) needs to be modified as [10] [26],

$$I=I_s\left(\frac{G}{1000}\right)\left\{1-\frac{e^{\alpha V}-1}{e^{\alpha V_o}\left(\frac{G}{1000}\right)-1}\right\} \tag{3.6}$$

Figure 3.14 shows the current voltage curves for the *Powerfilm* solar cells for three different values of solar irradiation based on Equation (3.6) and on [15].

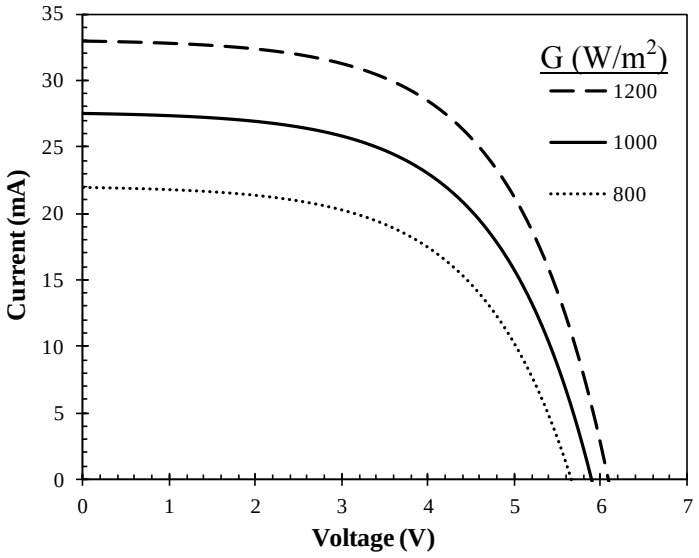

Figure 3.14: Current voltage curves for solar irradiation of 1200, 1000 and 800 W/m^2 for *Powerfilm SP4.2-37* solar cells [15].

Chapter 4: Results and Discussion

4.1 WIND AND SOLAR RESOURCE ASSESSMENT

4.1.1 Wind resource

The wind resource at Austin, TX specifically at the Pickle Research Campus, The University of Texas at Austin is assessed by the anemometer and wind vane as described in Section 3.1. The wind speed results are typically plotted as histograms for a certain number of days as shown in Figure 4.1. The uncertainty in the wind speed is 0.22 m/s for wind speeds up to 4.5 m/s and is 5 % of the value for wind speeds higher than 4.5 m/s Another convenient way to show the wind speed and the wind direction is by use of a wind rose chart, generated by *WRPLOT View* as shown in Figure 4.2. The uncertainty in the wind direction measurements is 0.3 to 0.5 % of the measured value.

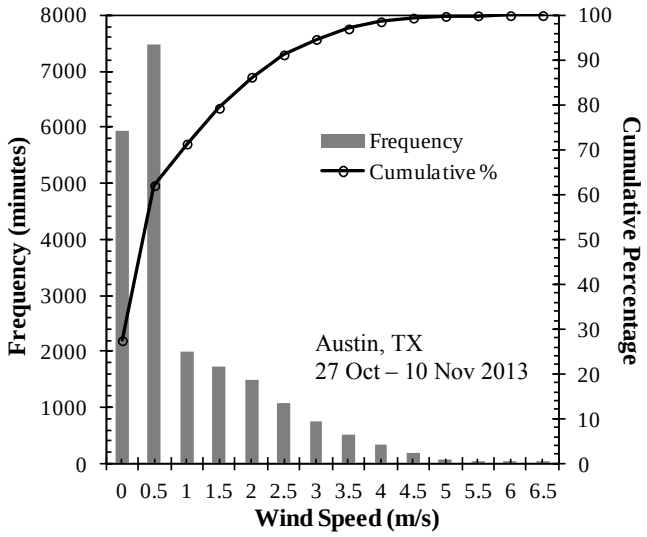

Figure 4.1: Wind speed histogram and cumulative percentage for a 15 day period of 27 Oct – 10 Nov 2013 at Austin, TX using measured data.

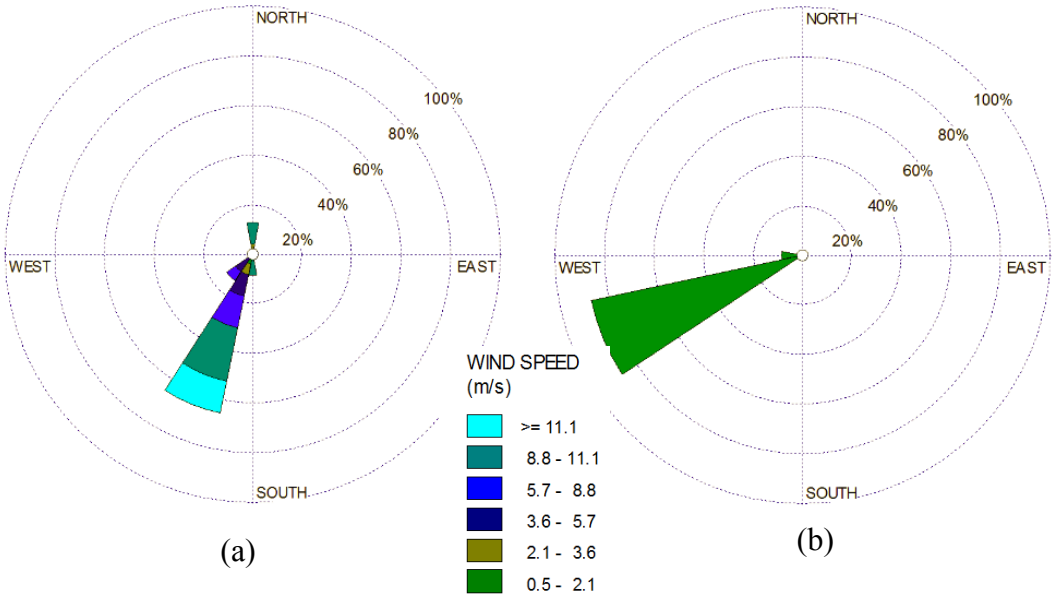

Figure 4.2: Wind Rose charts for 11 Oct 2013 at Austin TX, based on (a) historical TMY3 data and (b) the measured data

The data collected by the weather station in real time may not be sufficient enough to represent the statistical variability of weather at the given location. To solve this, Typical Meteorological Year (TMY) data based on statistical averaging of 30 years of weather data at a given location is useful. In particular, TMY 3 data deals with the data collected over the years 1991 to 2010 [27]. The TMY 3 data for Austin can be used to give a statistical estimation of the wind resource at Austin TX. Figure 4.3 shows the histogram of the wind speed data based on TMY 3.

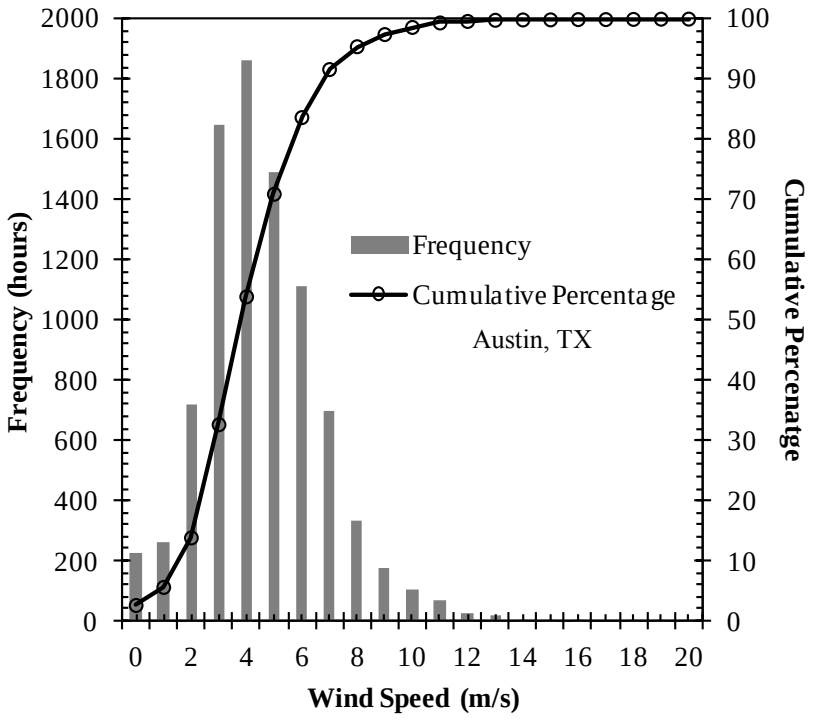

Figure 4.3: Wind speed histogram and cumulative percentage chart for Austin, TX based on Typical Meteorological Year 3 (TMY3) data [27]

4.1.2 **Solar resource**

The solar resource at Austin, TX specifically at the Pickle Research Campus, The University of Texas at Austin is assessed by the pyranometer as described in Section 3.1. As with the case of wind, histograms are used to visualize the data over a given number of days as shown in Figure 4.4. It is useful to consider only the instances of time in the histogram where the global horizontal radiation exceeds 100 W/m^2. At this value of the solar irradiation, it can be shown that the *Powerfilm* solar cells considered for the experiment gives 5 % of the rated power output of 92.4 mW. We define this as the threshold for the useful hours of the days where non negligible solar power can be produced with the given solar cells. Figure 4.5 shows that TMY3 data can be used for statistical estimation of the solar resource at Austin TX.

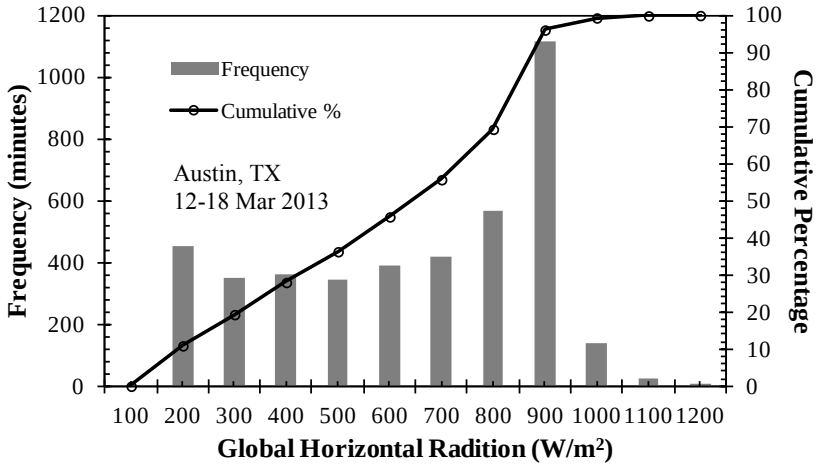

Figure 4.4: Global Horizontal Radiation histogram and cumulative percentage chart for 12- 18 Mar 2013 at Austin, TX using measured data for hours where Global Horizontal Radiation exceeds or equals 100 W/m^2

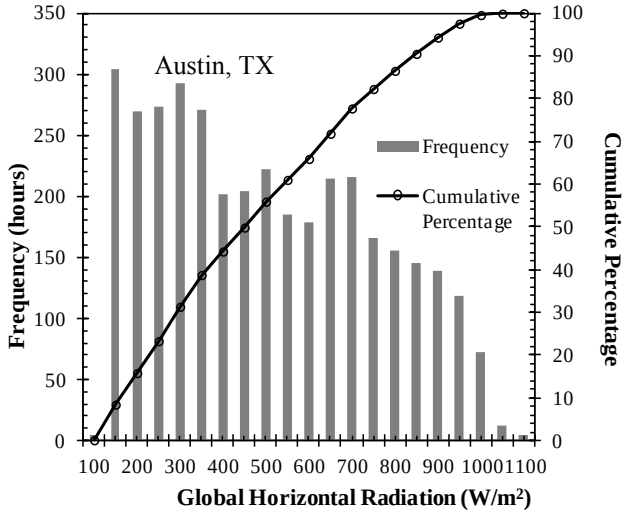

Figure 4.5: Global Horizontal Radiation histogram and cumulative percentage chart for 3650 hours of a Typical Meteorological Year 3 (TMY3) where Global Horizontal Radiation exceeds or equals 100 W/m^2 at Austin, TX

4.2 WIND POWER

As a first step to quantify the power output of the wind turbine, we aim to track the variation of the output DC voltage of the *Aurora* rectifier in open circuit, with wind speed and check if the 50 V threshold for grid tie in is achieved at wind speeds of 3-4 m/s. This is also tied in to the concept of cut in speed of wind turbines. This is the wind speed at which the turbine is able to supply useful power. Most turbines have cut in speeds of 3-4 m/s [10][28].

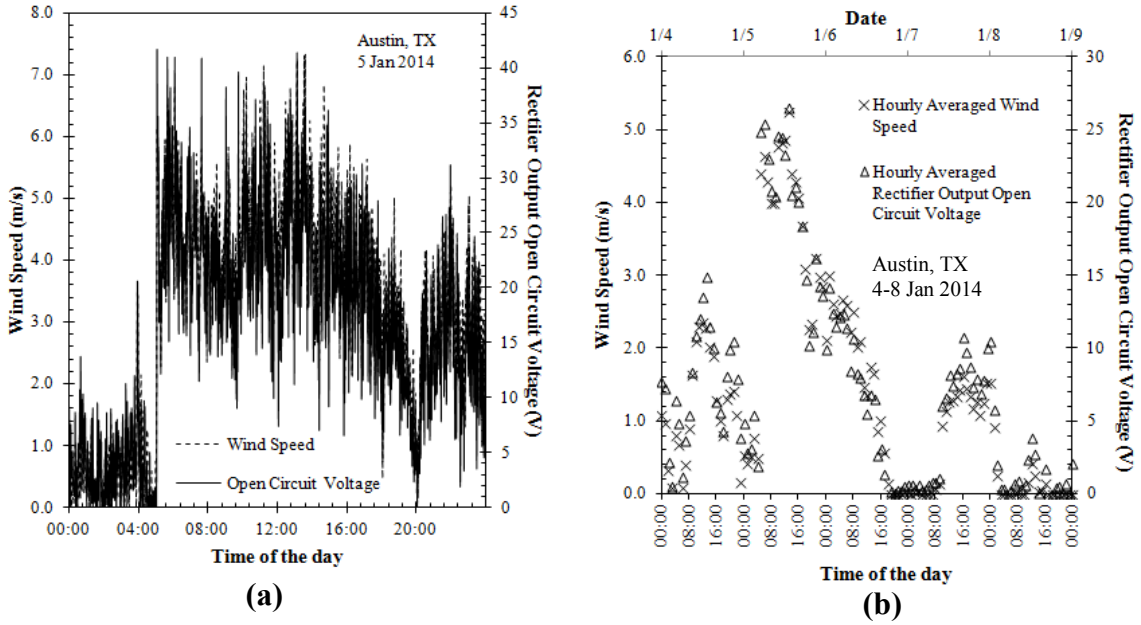

Figure 4.6: Wind speed with rectifier output open circuit voltage at Austin, TX for (a) 5 Jan 2014 and (b) for 4 Jan -8 Jan 2014

Figure 4.6 clearly shows that for wind speeds up to 7.5 m/s , the rectifier is un able to reach the 50 V threshold limit for grid tie in to be activated.

Figure 4.7 shows the cumulative percentage of the wind speed and the rotational speed of the turbine for 4-8 January 2014 respectively. The rotational speed of the turbine was back calculated from the generator specifications using the open circuit DC voltage [22].

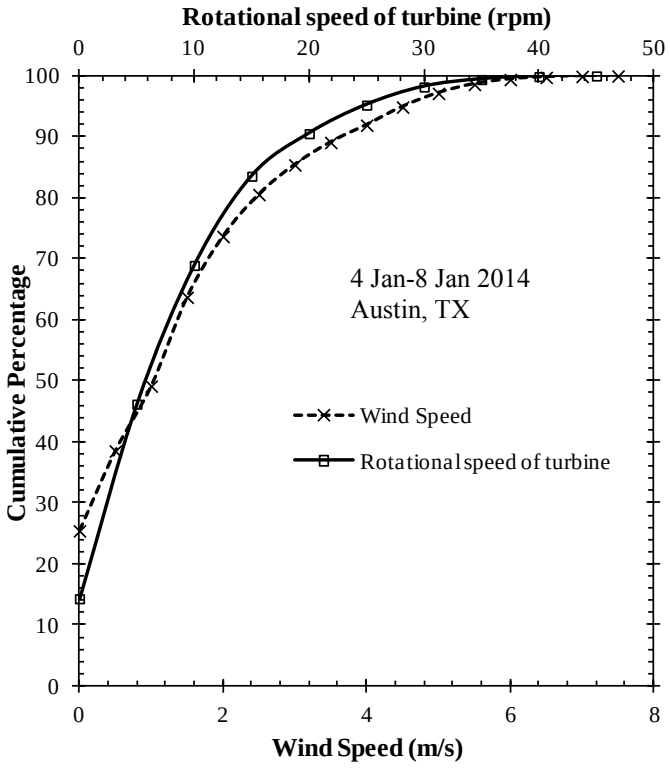

Figure 4.7: Cumulative percentage charts for wind speed and rotational speed of the turbine at Austin TX from 4-8 Jan 2014.

From Figure 4.7 a relationship between the wind speed V_{wind} in m/s and the rotational speed of the turbine $RPM_{turbine}$ in rpm is found to be

$$RPM_{turbine} \approx 5.3V_{wind}, V_{wind} \leq 7.5 m/s \tag{4.1}$$

As discussed in Section 3.2, if the minimum DC voltage to be supplied to the inverter for grid tie in is 50 V, the corresponding rms value of the 3 phase AC voltage supplied by the generator is around 37 V in open circuit.

With a cut in speed of 3-4 m/s in mind, we thus aim to find generators which can generate a 3 phase AC rms voltage of 37 V at wind speeds of around 3-4 m/s (which

correspond to turbine rotational speeds of 16-21 rpm, using Equation (4.1), so that grid tie in can be activated.

Figure 4.8 shows the open circuit 3 phase rms AC voltage with the rotational speed for the following three generators [22][29]:

1) *Air Boss 1400-96 V* (the current generator, manufactured by *AERCO)*
2) *Air Boss 1400-240 V* (manufactured by *AERCO)*
3) *Ginlong GL PMG 1800* (manufactured by *Ginlong)*

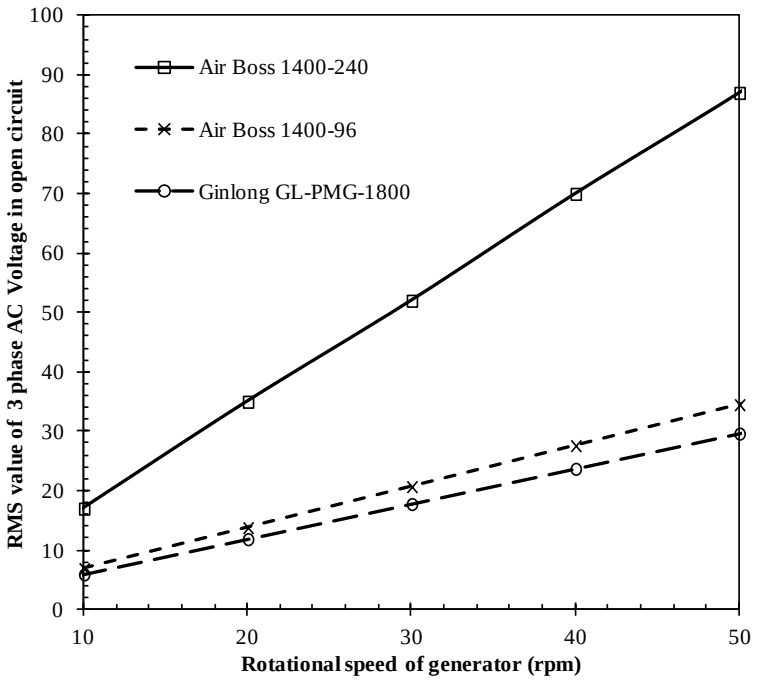

Figure 4.8: Open circuit 3 phase rms AC voltage vs rotational speed for the three generators considered

Figure 4.8 shows clearly that in order to get 37 V rms 3 phase AC voltage at a rotational speed of around 16-21rpm, the best choice is the *Air Boss 1400-240 V*. The other two generators give an output less than half of the *Air Boss 1400-240 V*. Thus it is

strongly recommended to replace the current generator *Air Boss 1400-96 V* with the *Air Boss 1400-240 V*.

Using the coefficient of performance data for a vertical axis wind turbine from literature [30] and the TMY3 data for wind speed at Austin TX, the monthly wind energy output of the turbine can be estimated for both the *Air Boss 1400-96 V* and *Air Boss 1400-240 V* generators. The results are shown in Figure 4.9

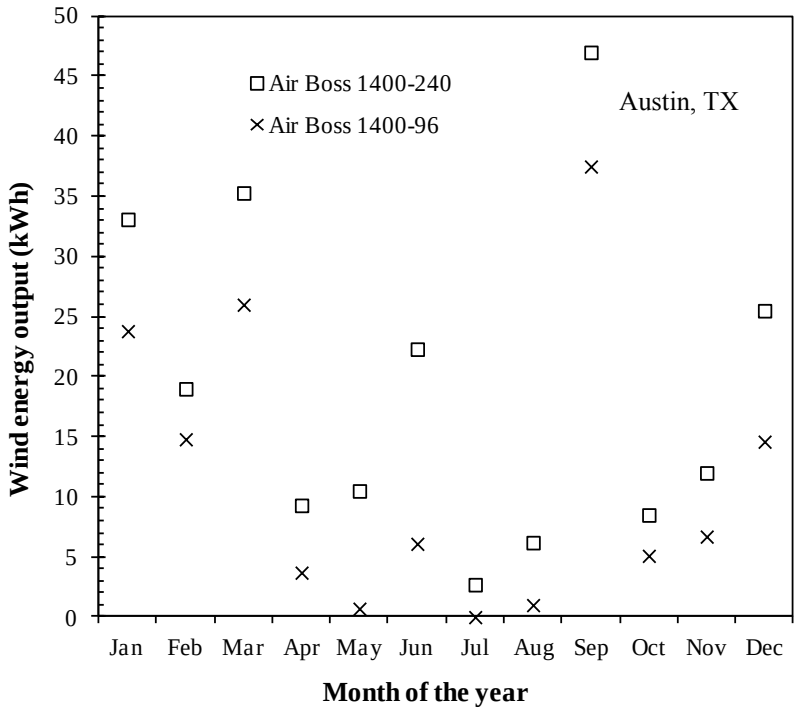

Figure 4.9: Estimated monthly wind energy output of the Marilyn turbine for the Air Boss 1400-96 V and Air Boss 1400-240 V generators at Austin TX.

As can be inferred from Figure 4.9, the estimated yearly wind energy output using the *Air Boss 1400-240 V* generator is 230 kWh and using the *Air Boss 1400-96 V* is 140

kWh. Thus a strong case is made to replace the Air Boss 1400-96 V with the Air Boss 1400-240 V generator.

4.3 SOLAR POWER

Figure 4.10 shows the top view of the turbine rotor and the blue regions represent the Solar sections as described in Section 3.3 . In this analysis, the solar radiation incident on these regions was considered at 1 pm on July 23 in Austin, TX based on TMY3 data. Figure 4.10 also shows the orientation of the turbine rotor, ψ, at zero degree. The orientation, ψ, is defined from the axis and positive in the anti-clockwise direction.

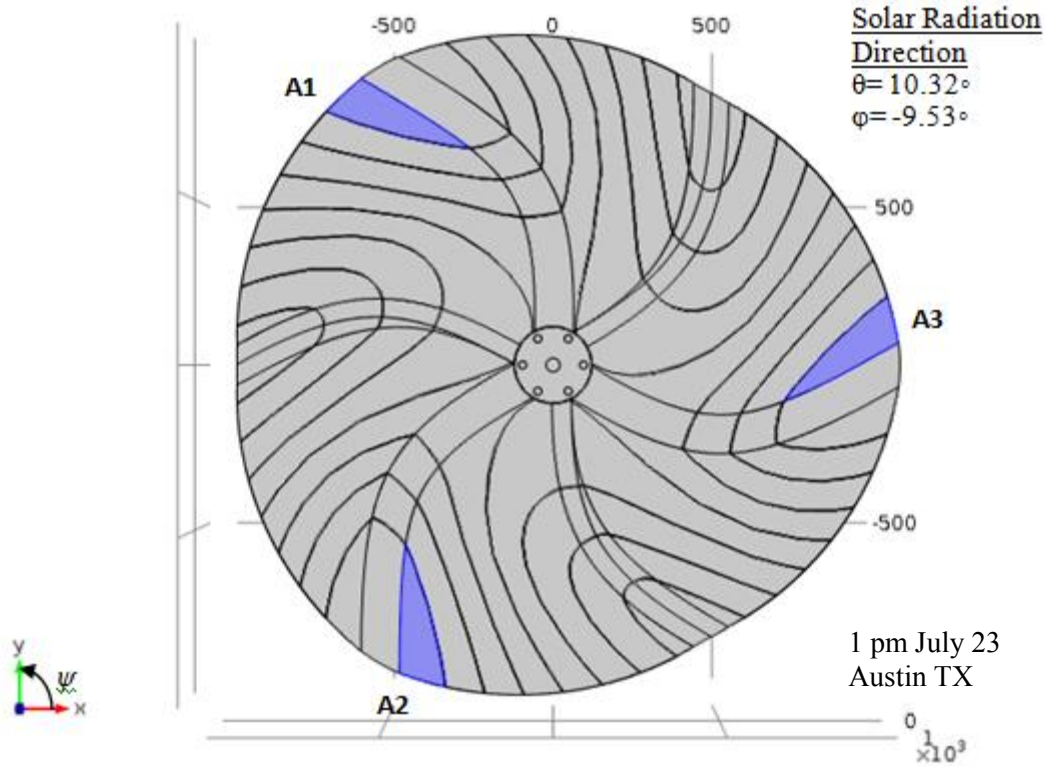

Figure 4.10: Top view of the *Marilyn* turbine. Solar sections are illustrated in blue as A1, A2 and A3 on the turbine rotor at the orientation, ψ, of zero.

The finite element analysis software, *COMSOL*, was used to estimate the average solar irradiation on regions A1, A2 and A3 at different orientations of the turbine rotor, ψ as done by Taylan [31]. For the sake of brevity we consider the case where all the solar cells are connected in series.

In the most general case, each of the three solar patches receives different normal total solar radiation and hence the solar cells have different *IV* curves. A resistor, R_{load}, was considered that was connected in parallel to this series combination to represent the

load. As the current was the same for all the solar cells, the current corresponded to the solar cell receiving the least amount of solar radiation. Thus, this configuration was current limited. Specifically, for a given orientation ψ, there exists a minimum resistance below which the current as required by Ohm's Law would exceed the short circuit current of the solar cell receiving the least amount of solar radiation.

Equation (3.6) can be rearranged to get V as function of I as,

$$V = \frac{1}{\alpha} ln \left[1 + \left\{ 1 - \frac{I}{I_s \left(\frac{G}{1000} \right)} \right\} \left\{ e^{\alpha V_o} \left(\frac{G}{1000} \right) - 1 \right\} \right] \tag{4.2}$$

If a number of solar cells are considered in series with the resistor R_{load}, the current can be expressed as,

$$I = \frac{\sum V_i}{R_{load}} = \frac{1}{R_{load} \alpha} \sum ln \left[1 + \left\{ 1 - \frac{I}{I_s \left(\frac{G_i}{1000} \right)} \right\} \left\{ e^{\alpha V_o} \left(\frac{G_i}{1000} \right) - 1 \right\} \right] \tag{4.3}$$

where G_i is the solar radiation incident on the i^{th} solar cell, which is a function of the orientation ψ. Equation (4.3) was iteratively solved in *MATLAB* to get the value of I.

Figure 4.11 shows the power of the solar cell section, P (which equals $I^2 R_{load}$) versus R_{load} as a function of the orientation, ψ. The orientation in Figure 4.11 is given from 0 to 110 degrees as the geometry of the turbine rotor is symmetrical with respect to 120 degrees.

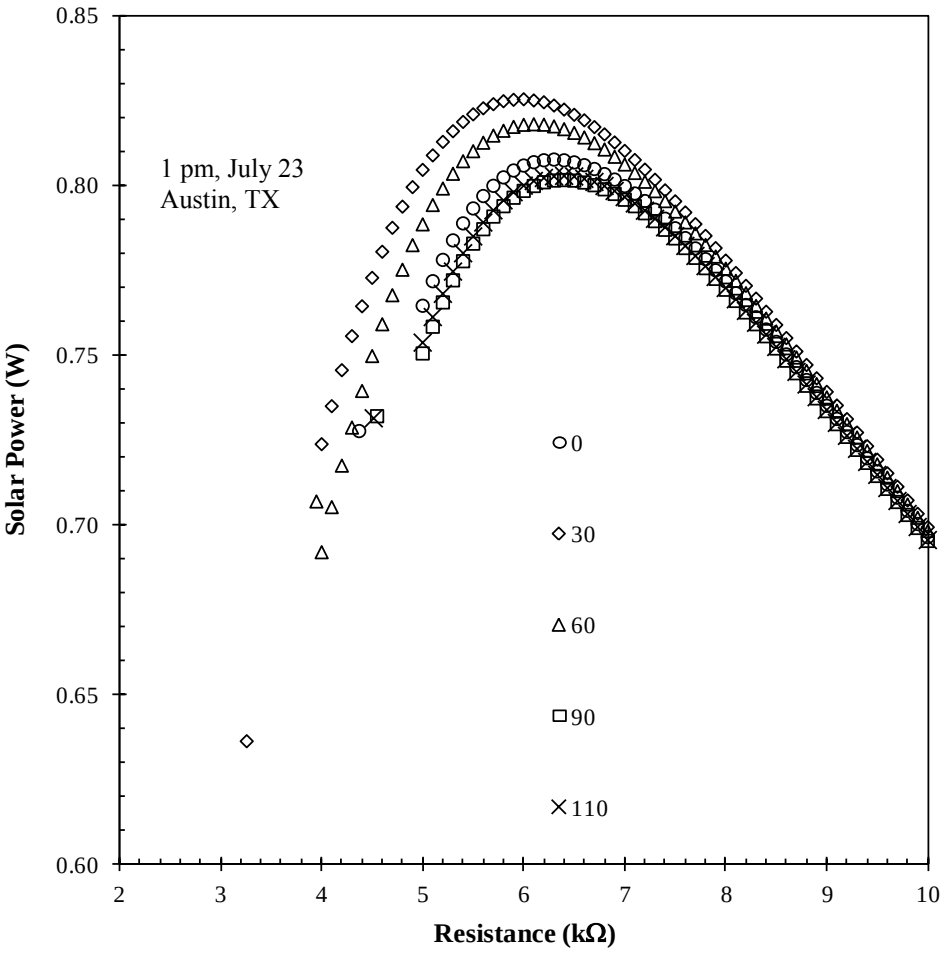

Figure 4.11: Solar power as a function of resistance at different orientations of the turbine when all solar cells were connected in series.

Figure 4.11 shows that the minimum resistance that can be connected to the series combination varies with the orientation. We also observe that the minimum resistance that works for all orientations was about 5.2 kΩ.

Figure 4.11 also shows that the variation of solar power, P with orientation ψ is less significant than the variation with the resistance of the load R_{load}. This leads us to

Figure 4.12 that indicates the variation of Solar Power P with the resistance of the load R_{load} from 7 am to 7 pm on 23 July based on TMY3 data for zero orientation ψ.

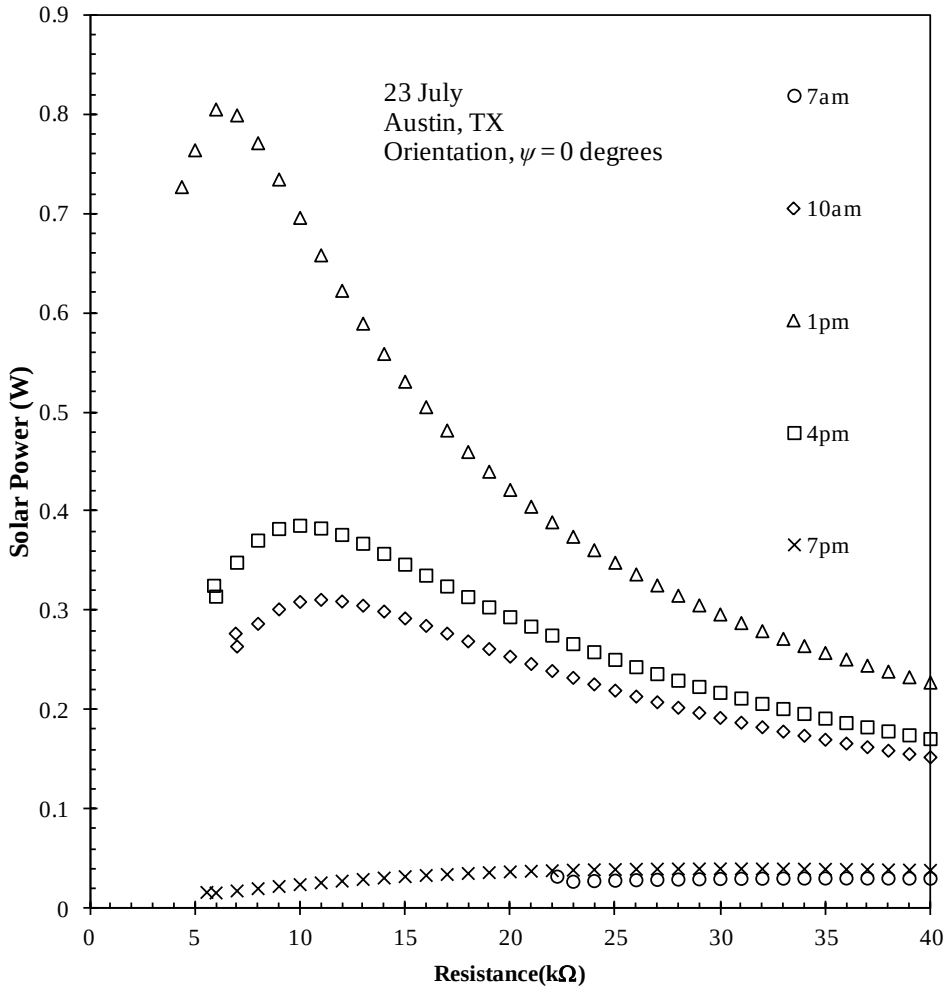

Figure 4.12: Variation of solar power with resistance from 7 am to 7 pm on 23 July based on TMY3 data

It is useful to compare the power obtained by these solar cells P mounted on the rotating surface to that obtained by the same number of cells if they were laid horizontal on the ground, called the Maximum theoretical power $P_{thr,max}$. Figure 4.12 shows the

resistance at which maximum power is obtained changes with the hour of the day. The power corresponding to this resistance at each hour is defined as the Maximum power with optimal resistance $P_{opt,max}$. We define connection efficiency η_{conn} as

$$\eta_{conn} = \frac{P}{P_{thr,max}} \tag{4.4}$$

Figure 4.13 shows the Maximum theoretical power $P_{thr,max,}$, the Maximum power with optimal resistance $P_{opt,max}$ and the power obtained at constant resistance of 25 kΩ, P from 7 am to 7 pm on 23 July. Figure 4.14 illustrates the corresponding connection efficiency. It is clear that the connection efficiency is the least in the hours with maximum solar irradiation i.e. 12-2 pm. This compromise in the performance of the solar cells is quite similar to the effects of partial shading on flat solar panels as discussed by Mazumadar *et al* [32] and Nguyen *et al* [33].

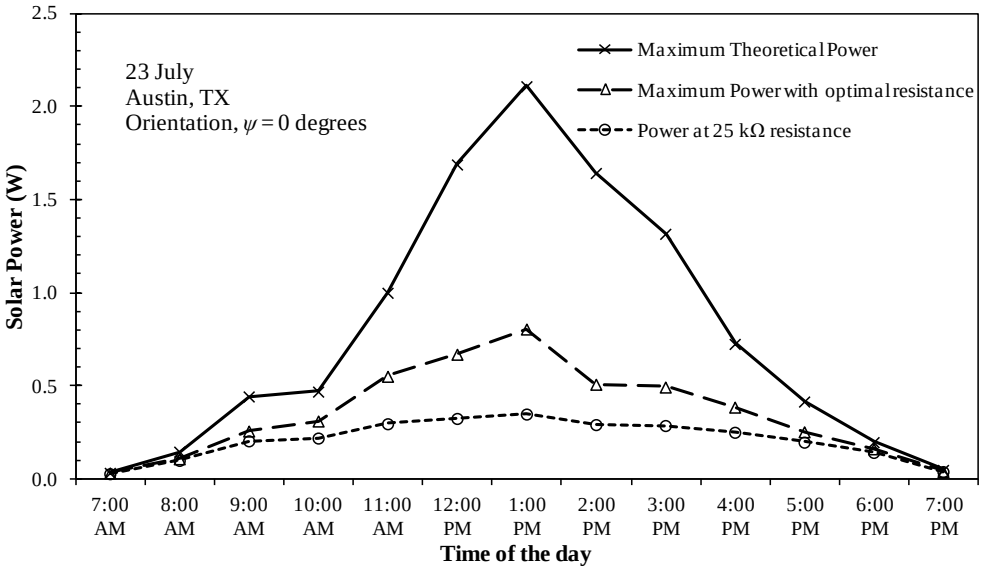

Figure 4.13: Variation of the Maximum theoretical power, the Maximum power with optimal resistance and the power obtained at constant resistance of 25 kΩ from 7 am to 7 pm on 23 July at Austin TX

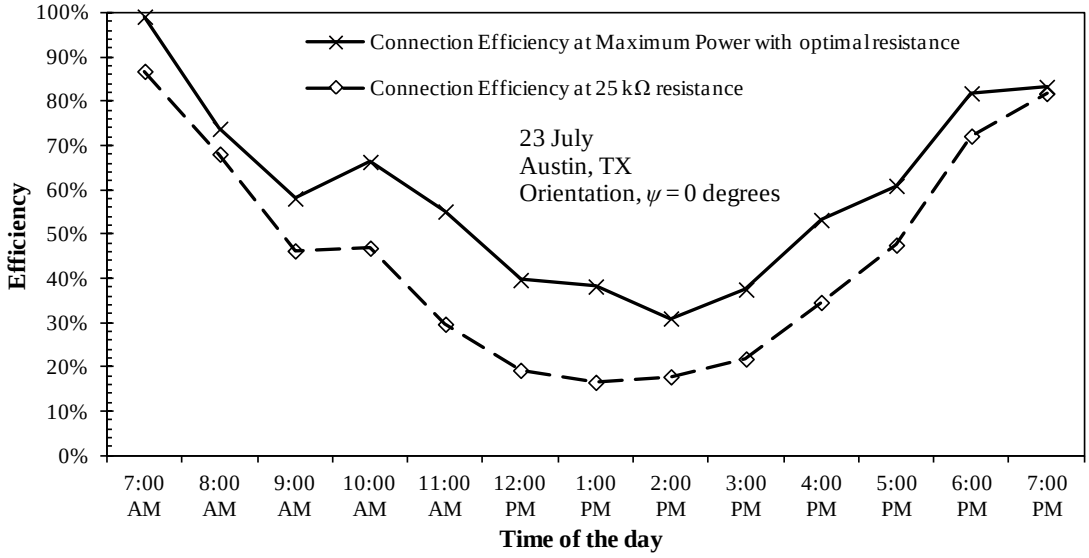

Figure 4.14: Variation of the connection efficiency at the case of Maximum theoretical power and the Maximum power with optimal resistance from 7 am to 7 pm on 23 July at Austin TX

A conservative estimate for the solar power obtained yearly if the entire top surface were covered with solar cells is attempted. An yearly estimate of the solar irradiation is obtained [31] and the resulting power is multiplied by the lower bound of the connection efficiency (approximately 20 %) and the solar cell efficiency. *EMPA*, Switzerland has manufactured flexible CIGS solar cells of up to 20 % efficiency. Taking this efficiency into account, Figure 4.15 shows the resulting solar energy output plotted for every month of the year and compared with the wind energy output.

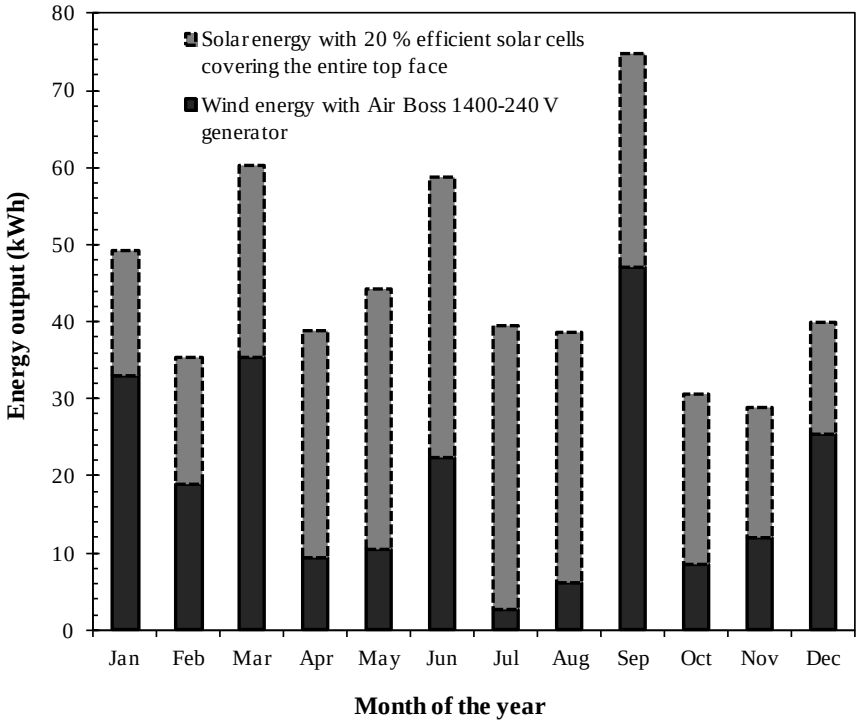

Figure 4.15: Monthly wind and solar energy output (conservative) with the Air Boss 1440-240 V generator and 20 % efficient solar cells covering the entire top face of the *Marilyn* turbine rotor.

Thus to summarize, in the above scenario, on an average we get about 240 kWh wind energy and about 310 kWh from solar energy for an year at Austin TX

Chapter 5: Conclusion and Recommendations

5.1 SUMMARY

This thesis analyzed the power production form wind and solar energy when solar cells are integrated on the surface of the *Marilyn* wind turbine. The study mainly includes (i) Suggestion of an alternative generator to the current one used and analysis of the yearly wind energy output as a result (ii) Analysis of the yearly solar energy output for the case when 20 % efficient flexible solar cells cover the entire top surface of the turbine.

- The *Air Boss* 1400-96 V, the current generator used, may be replaced by the *Air Boss* 1400-240 V to ensure that the grid tie in begins at wind speeds of 3-4 m/s The corresponding yearly wind energy output is 240 kWh on an average with the months of March and September being the most productive.
- Using flexible 20 % efficient CIGS solar cells manufactured by SMPA, Switzerland to cover the entire top surface of the turbine, a conservative estimate for the yearly solar power on an average is 310 kWh with the most productive months being June and July. It turns out that in these months the wind energy output is the least, leading to the conclusion that the solar energy compensates for the shortfall of wind energy in these months.
- The total yearly wind and solar energy output is 550 kWh which is around 5 % of the current annual residential electricity consumption in the United States

5.2 RECOMMENDATIONS FOR FUTURE RESEARCH

The presented thesis opens several questions to be answered through further research. Following are the recommended studies that can be performed for further understanding of the discussed subject:

- The use of a Maximum Power Point Tracker (MPPT) can be used to enhance the power obtained from the solar cells. The MPPT can be used to choose the optimal resistance for extracting the maximum solar power based on the solar irradiance at the given time. It is expected the use of MPPT can significantly boost the yearly solar energy output to beyond the current conservative estimate of 300 kWh. Further research along these lines can give a better understanding on enhancing the solar power output.

Appendix: MATLAB code for estimating solar power production by all solar cells in series

Following is the main code for estimating the solar power production from the solar cells on all the three solar sections connected in series at 23 July 1 pm Austin TX from the so . The inputs of this code are: solar irradiation on the top surface of the *Marilyn* rotor at 1 pm for 0-120 degree orientation from *COMSOL* simulations, solar cell parameters and the resistance across the solar cells. This code generates the power production for a range of resistances at each orientation.

```
a=0.941155;
Is=0.0275;
Vo=5.9;
Isa=zeros(37,3);
I=zeros(37,1);
filename='Airfoil Solar Irrad Areas 23 July 1 pm.xlsx';
M=xlsread(filename);

G=zeros(37,4);
step=1e2;
final=1e4;
initial=3*1e3;
P=zeros(37*((final-initial)/step),3);
l=1;

for j=1:37
    G(j,1)=M(j+4,1);
    for i=2:4
        G(j,i)=M(j+4,i+5);
        Isa(j,i-1)=Is*G(j,i)*0.001;
    end

    I(j)=min(Isa(j,:));
    v=0;

    for i=1:3
        P1=1-I(j)/Isa(j,i);
        P2=exp(a*Vo)*(G(j,i+1)*0.001)-1;
        v=v+(1/a)*7*log(1+P1*P2);
    end
```

```
        Rmin=v/I(j);
        kg=I(j);
        k=0;
        n=ceil(Rmin/1e3);
        P(l,1)=Rmin;
        P(l,2)=v*I(j);
        P(l,3)=(j-1)*10;
        l=l+1;

        for R=n*1e3:step:final;
            while abs(kg-k)>=1e-4 && kg>=0
                kg=kg-1e-6;
                k=0;
                for i=1:3
                    P1=1-kg/Isa(j,i);
                    P2=exp(a*Vo)*(G(j,i+1)*0.001)-1;
                    k=k+(1/R*a)*7*log(1+P1*P2);
                end
            end

            P(l,1)=R;
            P(l,2)=R*k^2;
            P(l,3)=(j-1)*10;
            l=l+1;
            kg=I(j);
            k=0;
        end
    end
```

Bibliography

[1] Renewable Energy Policy Network for the 21st Century, "Renewables 2013: Global Status Report," 2013.

[2] U.S. Energy Information Association, "How much electricity does an American home use?" [Online]. Available: http://www.eia.gov/tools/faqs/faq.cfm?id=97&t=3.

[3] U.S. Energy Information Association, "How much carbon dioxide is produced per kilowatthour when generating electricity with fossil fuels?" [Online]. Available: http://www.eia.gov/tools/faqs/faq.cfm?id=74&t=11.

[4] H. Riegler, "HAWT versus VAWT," *Renewable Energy Focus*, no. August, pp. 44–46, 2003.

[5] J. R. Bumby, N. Stannard, and R. Martin, "A Permanent Magnet Generator for Small Scale Wind Turbines," 2006.

[6] T. Ackermann and L. Söder, "An overview of wind energy-status 2002," *Renew. Sustain. Energy Rev.*, vol. 6, no. 1–2, pp. 67–127, Jan. 2002.

[7] M. Laidi, S. Hanini, B. Abbad, and N. K. Merzouk, "Study of a Solar PV-Wind-Battery Hybrid Power System for a Remotely Located Region in the Southern Algerian Sahara : Case of Refrigeration," *J. Technol. Innov. Renew. Energy*, no. 213, pp. 30–38, 2012.

[8] Renewable Energy Solutions LLC, "Breakthrough Small Wind Power Systems for Commercial, Utility and Residential Use." [Online]. Available: http://reswindsolutions.com/index.html.

[9] S. Eriksson, H. Bernhoff, and M. Leijon, "Evaluation of different turbine concepts for wind power," *Renew. Sustain. Energy Rev.*, vol. 12, no. 5, pp. 1419–1434, Jun. 2008.

[10] J. Duffie and W. Beckman, *Solar Engineering Of Thermal Processes*. Wiley, 2006.

[11] M. Ragheb and R. Ragheb, Adam M; Carriveau, "Wind Turbines Theory - The Betz Equation and Optimal Rotor Tip Speed Ratio," in *Fundamental and Advanced Topics in Wind Power*, vol. 1, no. 1, 2011.

[12] E. de Vries, “Close up - Vestas V164-8.0 nacelle and hub,” *Wind Power Monthly*, 2013. [Online]. Available: http://www.windpowermonthly.com/article/1211056/close---vestas-v164-80-nacelle-hub.

[13] Clean Energy Action Project, *Alta Wind Energy Center*, no. 100. 2012.

[14] First Solar, “Agua Caliente Solar Project Datasheet,” 2012.

[15] Powerfilm, “Powerfilm Solar Cells IV curve.” .

[16] M. Ranaboldo, B. D. Lega, D. V. Ferrenbach, L. Ferrer-Martí, R. P. Moreno, and A. García-Villoria, “Renewable energy projects to electrify rural communities in Cape Verde,” *Appl. Energy*, vol. 118, pp. 280–291, Apr. 2014.

[17] LI-COR Biosciences, “Certificate of Calibration for LI-COR Sensor Pyranometer Model Number : LI-200,” 1995.

[18] Inspeed, “Inspeed Vortex ‘Pole Mount’ Anemometer.”[Online]. Available: http://www.inspeed.com/anemometers/Pole_Mount_Anemometer.asp.

[19] Inspeed, “Inspeed E-VANE Electronic Wind Direction Sensor.” [Online]. Available: http://www.inspeed.com/wind_speed_direction/Vane.asp.

[20] LI-COR Biosciences, “Principles of Radiation Measurement,” 2008.

[21] Campbell Scientific Inc, “CR10X Specifications,” 2004.

[22] American Energy Research Corporation, “Air Boss Generator Performance Data,” 2012.

[23] Power One, *Wind Inverters Installation and Operator’s manual*, no. 2.2. 2009.

[24] D. Juan and M. Rashid, “Chapter 12: Three phase controlled rectifiers,” in *Power Electronics Handbook*, 2011, pp. 205–266.

[25] National Instruments, “Part II – Photovoltaic Cell I-V Characterization Theory and LabVIEW Analysis Code,” pp. 5–8, 2012.

[26] E. Peng and H. Berberoğlu, “Temperature and Irradiance Dependence of a Dye Sensitized Solar Cell With Acetonitrile Based Electrolyte,” *J. Sol. Energy Eng.*, vol. 134, no. 1, p. 011011, 2012.

[27] S. Wilcox and W. Marion, “Users Manual for TMY3 Data Sets,” 2008.

[28] T. Burton, D. Sharpe, N. Jenkins, and E. Bossanyi, *Wind Energy Handbook*. Wiley, 2001.

[29] Ginlong Technologies, *Ginlong Technologies GL-PMG-1800 Characteristics*. .

[30] Masahiko Suzuki Hideto Taniguchi, “An experimental vertical-axis wind turbine system with Bellshion blades,” 2008.

[31] O. Taylan, “Integration of solar cells to Marilyn rotor,” 2012.

[32] P. Mazumdar, P. N. Enjeti, and R. S. Balog, “Analysis and design of smart PV modules,” *2013 Twenty-Eighth Annu. IEEE Appl. Power Electron. Conf. Expo.*, pp. 84–91, Mar. 2013.

[33] D. Nguyen and B. Lehman, “An Adaptive Solar Photovoltaic Array Using Model-Based Reconfiguration Algorithm,” *IEEE Trans. Ind. Electron.*, vol. 55, no. 7, pp. 2644–2654, 2008.

Vita

Mahesh Venkatesan received a Bachelor of Technology in Mechanical Engineering from the Indian Institute of Technology Roorkee in May 2011. His bachelor thesis was on the active vibration control of a cantilever beam with piezoelectric sensors and actuators. He worked for a year at Royal Dutch Shell as a Project Risk Analyst, before beginning graduate study in the Thermal/Fluid Systems track of Mechanical Engineering department at The University of Texas at Austin in the fall of 2012. In January 2013, he began his research with Dr. Halil Berberoglu in the Solar Energy and Renewable Fuels Laboratory, where his study was focused on the experimental and theoretical analysis of a novel vertical axis wind turbine with solar cell integration.

Permanent address: mak.261089@gmail.com

This thesis was typed by the author.